Fryer, P., Pearce, J. A., Stokking, L. B., et al., 1990
Proceedings of the Ocean Drilling Program, Initial Reports, Vol. 125

9. SITE 781[1]

Shipboard Scientific Party[2]

HOLE 781A

Date occupied: 11 March 1989

Date departed: 13 March 1989

Time on hole: 2 days, 15 hr, 30 min

Position: 19°37.91′N, 146°32.56′E

Bottom felt (rig floor; m; drill-pipe measurement): 4431.7

Distance between rig floor and sea level (m): 11.10

Water depth (drill-pipe measurement from sea level: 4420.6

Total depth (rig floor; m): 4681.7

Penetration (m): 250.0

Number of cores: 27

Total length of cored section (m): 247.0

Total core recovered (m): 39.62

Core recovery (%): 16

Oldest sediment cored:
Depth (mbsf): 250.0
Nature: vitric silty clay and vitric sandy silt
Earliest age: late Miocene(?)–early Pliocene(?)

Hard rock:
Depth (mbsf): 67.3
Nature: basalt (flow or sill)
Measured velocity (km/s): 3.9–5.3

Principal results: Site 781 is situated about 7 nmi northwest of the summit of Conical Seamount on the outer-arc high of the Mariana forearc basin, about midway between the active Mariana arc and the trench axis. The principal objectives of this site were to fulfill the unachieved aims of the seamount flank Sites 778 and 779, namely to study the sediments and basement beneath the serpentinite seamount and hence to determine the age range of serpentinite diapirism and to characterize the type of crust into which the serpentinite was intruded. We hoped that a site at the base of the seamount free of serpentine flows, as determined by SeaMARC II side-scanning sonar imagery, would achieve these objectives. Precise site selection was based on six-channel seismic records that showed a strong reflector, possibly basement, at about 60 mbsf, a feature that was confirmed by a short underway geophysical survey.

Hole 781A was drilled with an RCB, penetrating 250 m and recovering 39.6 m of core for a recovery rate of 16%. Most of the poor core recovery was in sediments below the basalt subunit that was encountered between 72.6 and 91.8 mbsf. One lithologic unit having three subunits was defined as follows:

1. Subunit IA (0–72.32 mbsf) comprises late Pliocene(?)–Holocene(?) diatom-radiolarian silty clay that grades downward into vitric silty clay and vitric clayey silt.
2. Subunit IB (72.32–91.80 mbsf) is a vesicular, porphyritic basalt.
3. Subunit IC (91.80–250 mbsf) comprises late Pliocene to early Pliocene vitric silty clay and vitric clayey silt.

These sediments exhibit structures indicative of deposition from gravity-driven mass flows and contain interstitial fluids that exhibit only small chemical deviations from seawater composition downhole. The basalt of Subunit IB, which corresponds to the reflector on the seismic records, is 13 to 25 m thick, is massive, and may be a near-surface sill or a lava flow and thus of Pliocene or later age. This basalt provides the first evidence for such recent magmatic activity in any extant intraoceanic forearc terrane. Its geochemical signature indicates an origin from the mantle wedge above the subduction zone, but we cannot be certain if the source of the magma lies some 100 km to the west, in the region of the active Mariana arc, or whether it represents a hitherto unknown source of magma within the forearc basin itself.

BACKGROUND AND SCIENTIFIC OBJECTIVES

The flank sites on Conical Seamount (Sites 778 and 779) had failed to achieve one of the main objectives of drilling at the seamount, that of penetrating basement material. Basement penetration was deemed necessary to determine the nature of the crustal material underlying Conical Seamount and to assess the extent of interaction of that country rock with fluids from the serpentinite diapir. A site was chosen low on the northwest flank of the seamount (Fig. 1) in an area shown by seismic-reflection profiles to have a strong reflector at a depth of about 100 mbsf (Fig. 2). SeaMARC II images of the region showed that Site 781 was near the base of the seamount (Fig. 3). That base may be defined by the change in sonic backscatter on the side-scanning sonar imagery from the circle of very low (light) backscatter, which also shows concentric ridges or fractures, to the higher backscatter region (darker mottled gray) indicative of normal sedimented seafloor surrounding the seamount.

Studies of the seismic-reflection data collected near this site (see "Underway Geophysics" chapter, this volume) show a series of small fault blocks in the vicinity of Site 781. Gravity data collected over the seamount during several previous surveys indicate the presence of a fracture zone striking northwest-southeast beneath the seamount (Newsom, unpubl. data). We hoped that drilling at Site 781 would also enable us to determine the possible timing of the faulting and also determine whether the tectonism responsible for the faulting was related in any way to the formation of the seamount.

Drilling at Site 781 was undertaken to enable us to investigate (1) the nature of the basement underlying the adjacent seamount, (2) the timing of emplacement of the serpentinite seamount, (3) the effects on the basement materials of diapir-related alteration, and (4) the interaction of seamount-related activity with local sedimentation and/or tectonic processes.

OPERATIONS

Transit to Site 781

Problems with Site 780 prevented deep penetration into the top of Conical Seamount, leaving some of the time allotted for that hole unused. To obtain samples of the sediment and

[1] Fryer, P., Pearce, J. A., Stokking, L. B., et al., 1990. *Proc. ODP, Init. Repts.*, 125: College Station, TX (Ocean Drilling Program).
[2] Shipboard Scientific Party is as given in the list of participants preceding the contents.

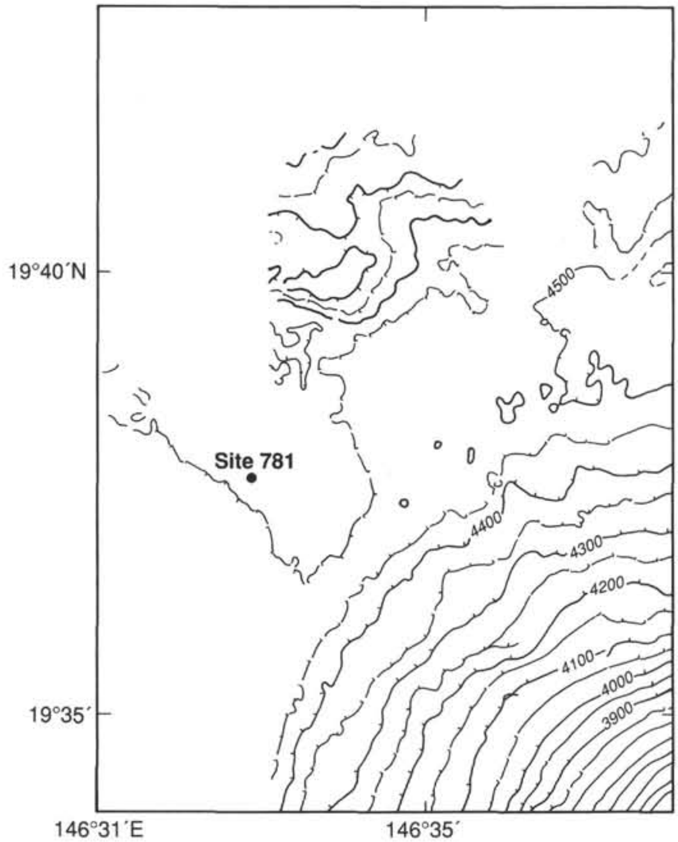

Figure 1. SeaBeam bathymetric contour map of the northwest flank of Conical Seamount (Stoffers, unpubl. data) showing the position of Site 781. Bathymetry in meters.

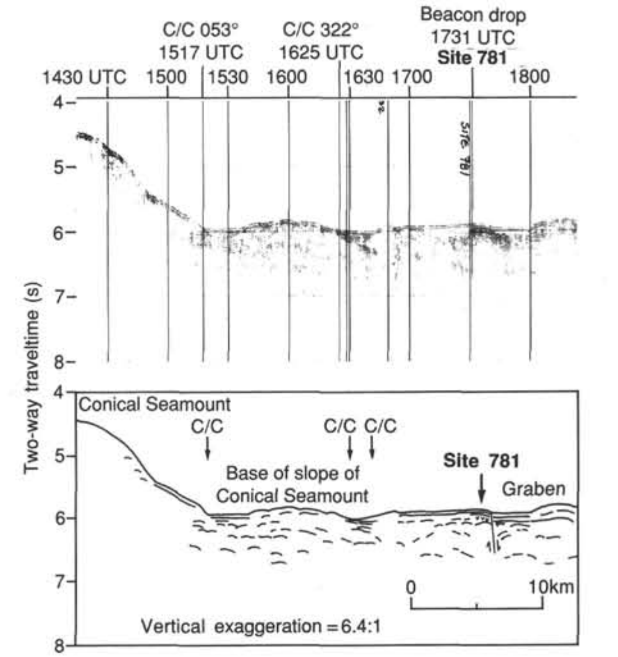

Figure 2. Seismic-reflection profile across Site 781, showing location of the beacon.

basement underlying the seamount, a site near the northern base of the seamount was proposed for drilling. Permission to drill to 250 mbsf was received from shorebased operations. The *JOIDES Resolution* was under way at 1345UTC, 10 March, and a seismic survey was conducted to determine the best location for the site. Site 781 was established by the dropping of a beacon at 1730UTC, 10 March.

Hole 781A

The vessel was positioned over a beacon, and the trip in with the drill pipe began at 2000UTC, 10 March. A standard RCB bottom-hole assembly (BHA) with a soft-formation bit was used to spud Hole 781A at 0315UTC, 11 March. The first RCB core retrieved had a recovery of 6.95 m of core to establish the mud line at 4420.6 m below sea level (bsl). No problems with the hole were encountered. A basalt was penetrated from 72.6 to 91.8 mbsf with little difficulty. Very little core was recovered from below the base of the basalt to the final depth of 250 mbsf. Hole 781A was abandoned after reaching the depth restriction at 250 mbsf. A total of 27 RCB coring runs were performed that recovered 39.6 m of core for a recovery rate of 16% (Table 1). Hole 781A and Site 781 officially ended at 0900UTC, 13 March, when the bit was back on deck and the *JOIDES Resolution* departed for the Izu-Bonin sites.

LITHOSTRATIGRAPHY

Lithologic Summary

Poor core recovery, particularly in the lower portion of the hole, limits both lithostratigraphic and biostratigraphic resolution; accordingly, only one lithologic unit has been defined for Site 781 (Table 2). Three subunits define two sedimentary sequences (Subunits IA and IC) and one vesicular-porphyritic basalt sequence (Subunit IB).

Unit I

Subunit IA: Cores 125-781A-1R-1, 0 cm, to 125-781A-8R-CC, 7 cm; depth, 0–72.32 mbsf.
Age: Holocene(?) to late Pliocene.

Subunit IA comprises two general lithologies: a brown to dark brown (7.5YR 2/2, 4/2, 4/4) diatom-radiolarian silty clay in the upper portion of the stratigraphic succession near the seafloor, transitional downhole to a gray to dark gray (5Y 5/1–5Y 4/1) vitric silty clay to vitric clayey silt. Diatoms (trace to 25%), radiolarians (trace to 15%), silicoflagellates, and sponge spicules (both trace to 10%) are the biosiliceous components. Calcareous biogenic components are nannofossils (trace to 35%) and foraminifers (trace to 15%); micrite (trace to 25%) in combination with these calcareous components defines calcareous clay and marl as a minor lithology (e.g., Core 125-781A-1R). Vitric particles increase in abundance downsection (trace to 55%) from Core 125-781A-4R to the base of the hole (Core 125-781A-27R). The admixture of vitric particles and microfossils form minor sedimentary lithologies in Subunit IA, such as radiolarian-bearing vitric silty clay, nannofossil silty marl, and biogenic-rich clay. Additional sediment components are opaque minerals (3%–25%), zoisite (3%–15%), serpentine (trace to 13%), feldspar and chlorite (both trace to 15%), lithic fragments (4%–10%), as well as olivine, pyroxene, epidote, and organic debris in amounts less than 5%.

Sedimentary structures indicative of deposition from gravity-driven mass flows suggest that a high proportion of the sediments in this subunit have been displaced. At least 19 turbidite sequences may be defined by basal clastic beds (mainly vitric-rich sands and silts) 0.5 to 40 cm thick (average about 1 cm) that frequently exhibit normal size-grading or cross-beds followed by faint laminae; this combination of sedimentary structures suggests Bouma units "a" through "c." Overlying homogeneous intervals of vitric-bearing clays suggest Bouma "d" units. Basal

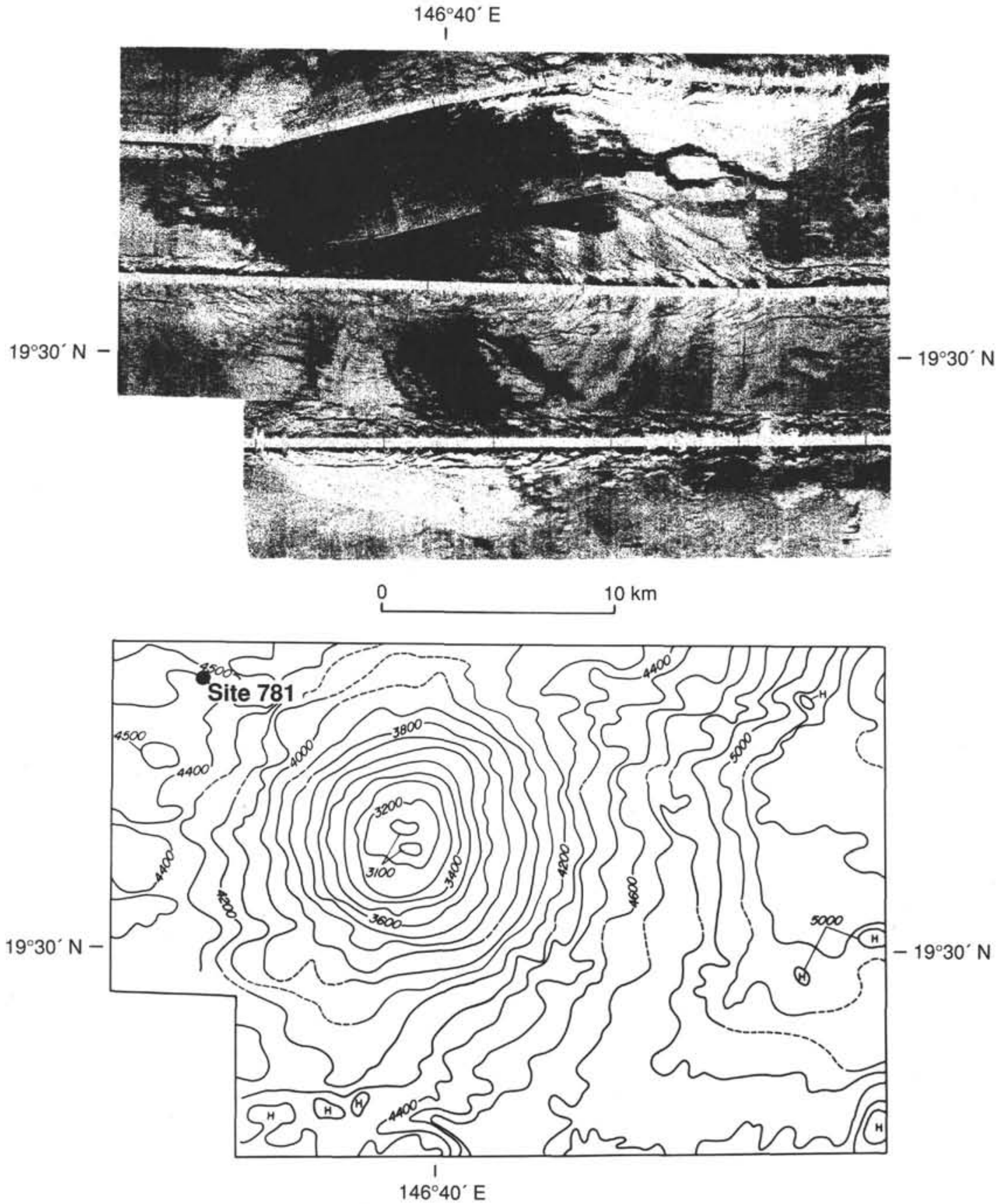

Figure 3. SeaMARC II side-scanning sonar imagery and bathymetry of the region around Site 781. Note the change in backscatter at the base of the seamount. Bathymetry in meters.

contacts are sharp and contain load casts where the basal clastic bed thickness is greater than about 2 cm. Upper contacts of some of these clastic beds have been disrupted by the injection of sands and silts into the overlying clays. Overall thicknesses of turbidite sequences vary between 1 and 180 cm, with an average in the range of 3 to 12 cm.

Subunit IB: Sections 125-781A-8R-CC, 8 cm, to 125-781A-10R-3, 112 cm; depth, 72.32–91.80 mbsf.
Age: late Pliocene.

Subunit IB is defined by a vesicular porphyritic basalt layer (see discussion in "Igneous and Metamorphic Petrology" section, this chapter). The upper sediment/basalt contact occurs in Section 125-781A-8R-CC at 7 cm. The lower basalt/sediment contact was not recovered, and a lower boundary for this subunit has been determined at 91.80 mbsf, between Cores 125-781A-10R and 125-781A-11R, by the decrease in drilling rotation/penetration rates.

Subunit IC: Sections 125-781A-14R-1, 0 cm, to 125-781A-27R-CC, 18 cm; depth, 120.7–250.0 mbsf.
Age: late Pliocene to early Pliocene.

Subunit IC is a sedimentary sequence that is poorly defined because of sparse core recovery. The first core from which sediment was recovered from this subunit is at 120.70 mbsf (Section 125-781A-14R-1), which defines the upper

Table 1. Coring summary for Hole 781A.

Core no.	Date (March 1989)	Time (UTC)	Depth (mbsf)	Length cored (m)	Length recovered (m)	Recovery (%)
1R	11	0420	0–6.9	6.9	6.95	101.0
2R	11	0615	6.9–16.4	9.5	0.00	0.0
3R	11	0745	16.4–25.9	9.5	0.00	0.0
4R	11	0925	25.9–35.4	9.5	0.77	8.1
5R	11	1040	35.4–44.9	9.5	0.20	2.1
6R	11	1220	44.9–54.5	9.6	6.91	72.0
7R	11	1330	54.5–64.5	10.0	4.41	44.1
8R	11	1520	64.5–72.6	8.1	2.85	35.2
9R	11	1950	72.6–82.3	9.7	3.75	38.6
10R	11	2345	82.3–91.8	9.5	2.58	27.1
11R	12	0130	91.8–101.4	9.6	0.00	0.0
12R	12	0300	101.4–111.1	9.7	0.01	0.1
13R	12	0415	111.1–120.7	9.6	0.00	0.0
14R	12	0545	120.7–130.4	9.7	0.06	0.6
15R	12	0700	130.4–140.0	9.6	0.01	0.1
16R	12	0820	140.0–149.6	9.6	0.13	1.4
17R	12	0950	149.6–156.3	6.7	0.00	0.0
18R	12	1150	159.3–168.9	9.6	0.02	0.2
19R	12	1315	168.9–178.6	9.7	0.00	0.0
20R	12	1500	178.6–188.2	9.6	0.00	0.0
21R	12	1630	188.2–197.9	9.7	0.58	6.0
22R	12	1800	197.9–207.6	9.7	0.15	1.5
23R	12	1950	207.6–217.3	9.7	0.02	0.2
24R	12	2100	217.3–226.9	9.6	0.14	1.5
25R	12	2215	226.9–236.5	9.6	0.16	1.7
26R	12	2330	236.5–246.0	9.5	0.54	5.7
27R	13	0145	246.0–250.0	4.0	9.38	234.0
Coring totals				247.0	39.62	16.0

limit of Subunit IC. Thus, a gap of 28.90 m exists between Subunits IB and IC (see Table 2) in which no sediment or rock was recovered, preventing accurate subunit description and boundary definition. However, rapid drilling and penetration rates imply unconsolidated sediment throughout both the subunit and the gap between the subunits. Sediments in Subunit IC are predominantly vitric silty clays and vitric clayey silts, with minor feldspar-rich vitric sands, silts, clays, and all permutations of the latter three textural categories. In addition to volcanic ash (in amounts from 12%–55%) and clays (8%–70%), the minerals and biogenic particles present are feldspar (7%–20%), zoisite and pyroxene (both trace to 10%), opaque minerals (5%–10%), epidote (2%–6%), lithic fragments (predominantly igneous) and serpentine (both trace to 5%), amphibole and olivine (both in trace amounts), micrite (5%–20%), calcareous nannofossils (5%–15%), foraminifers (trace to 5%), and radiolarians (trace). Colors are predominantly gray to dark gray (5Y 5/1 to 5Y 4/1–10YR 4/1), with some dark brown, very dark brown, and black (5YR 3/1, 7.5YR 2/2, 2/0).

Two angular pebbles of basalt were recovered in Core 125-781A-18R; smaller basalt granules are present in minor amounts in Cores 125-781A-16R, 12-781A-21R, 125-781A-24R, and 125-781A-26R. Vitric clay and silt containing basalt granules and clay clasts were recovered in Core 125-781A-27R, the last core at this site. We are still unclear as to whether this entire 9.7-m-long sediment sequence represents *in-situ* material, contaminants accumulated at the bottom of the hole, or both. Information from both drilling operations and sediment analyses implies that at least one-half of this core represents downhole contaminants.

BIOSTRATIGRAPHY

Evidence from calcareous nannofossils in Site 781 cores indicates that the sedimentary interval from Sample 125-781A-1R-1, 2 cm, to Sample 125-781A-7R-CC ranges in age from early to late Pleistocene; that Samples 125-781A-8R-CC, 125-781A-15R-CC, 125-781-16R-CC, 125-781A-18R-CC, and 125-781A-25R-CC are from the late Pliocene; and that the age of the sedimentary interval from Samples 125-781A-26R-CC to 125-781A-27R-CC is early Pliocene, even if mixed assemblages occur that reflect contamination or reworking. Evidence from foraminifers confines Sample 125-781A-21R-CC to late Pliocene and Sample 125-781A-27R-CC to earliest early Pliocene.

Calcareous Nannofossils

Poorly to well-preserved, rare to abundant nannofossil assemblages are present in the sediments overlying the basalt layer in Hole 781A. Samples 125-781A-1R, 2 cm, and 125-781A-1R-CC are late Pleistocene (Zone CN15) in age, on the basis of the occurrence of *Emiliania huxleyi*, *Gephyrocapsa oceanica*, *G. caribbeanica*, *Helicosphaera hyalina*, and *Ceratolithus telesmus*. Samples 125-781A-4R-CC and 125-781A-5R-CC are dated to middle/early Pleistocene (Subzone CN14a) by the occurrence of *Pseudoemiliania lacunosa*. Samples 125-781A-6R-CC, and 125-781A-7R-CC are dated as early Pleistocene (base of Subzone CN14a) from the occurrence of *Helicosphaera sellii* in Sample 125-781A-6R-CC and from the co-occurrence of this species with *Gephyrocapsa oceanica*. A few reworked nannofossils from the Miocene and/or from the Pliocene are also present.

Samples 125-781A-8R-CC and 125-781A-15R-CC contain a rare and poorly preserved nannofossil assemblage with *Pseudoemiliania lacunosa*, *Discoaster surculus*, *D. brouweri*, *D.* aff. *asymmetricus*, *D. pentaradiatus*, *Ceratolithus cristatus*, and *Calcidiscus macintyrei*. These age-diagnostic species together with the lack of *Discoaster tamalis* and *D. variabilis* indicate that the sample is late Pliocene (Subzone CN12b) in age. Reworked *Discoaster* aff. *saipanensis*, *D. deflandrei*, and *Sphenolithus* sp. of Eocene age are also present.

Samples 125-781A-16R-CC to 125-781A-25R-CC contain few or common and poorly preserved nannofossils characterized by the marker species *Pseudoemiliania lacunosa*, *Discoaster asymmetricus*, *D. tamalis*, and *D. variabilis*, which provide an age of late Pliocene (Zone CN12a) for these samples.

Sample 125-781A-26R-CC is latest early Pliocene in age (Zone CN11b) on the basis of the occurrence of *Discoaster tamalis* and *Pseudoemiliania lacunosa* together with *Reticulofenestra pseudoumbilica* and *Sphenolithus abies*.

Table 2. Lithologic units recovered at Site 781.

Lithologic unit/subunit	Cores	Depth (mbsf)	Dominant lithology	Stratigraphic age
IA	125-781A-1R-1, 0 cm to 125-781A-8R-CC, 7 cm	0 to 72.32	Diatom-radiolarian silty clay to vitric silty clay and vitric clayey silt	Holocene(?) to upper Pliocene
IB	135-781A-8R-CC, 8 cm to 125-781A-10R-3, 112 cm	72.32 to 91.80	Vesicular porphyritic basalt	upper Pliocene
IC	125-781A-14R-1, 0 cm to 125-781A-27R-CC, 18 cm	120.70 to 250.00	Vitric silty clay and vitric clayey silt	upper Pliocene to lower Pliocene

Sample 125-781A-27R, CC is characterized by an abundant and moderately preserved nannofossil assemblage. However, several zonal markers covering a range of zones are present. For example, *Amaurolithus delicatus*, *Ceratolithus acutus*, *C. armatus* and *Triquetrorhabdulus rugosus* (zonal markers of the early Pliocene) were found together with *Pseudoemiliania lacunosa*, *Discoaster tamalis*, and *D. asymmetricus* (first occurrence in late early Pliocene). This interval can be interpreted either as reworked, in which case it is late Pliocene in age, or, more probably, as contaminated from coring, which makes it early Pliocene.

Only solution-resistant coccoliths can be found in Sample 125-781A-4R-CC. The assemblage is typical of the Mesolytic Zone (Schneidermann, 1977). This zone lies about 500 m above the carbon compensation depth (CCD). The next sample (125-781A-5R-CC) is high in diversity and contains coccoliths that are not resistant to solution. Moreover, the presence of the genus *Pontosphaera*, an epipelagic taxon, might indicate that Sample 125-781A-5R-CC was deposited at a shallower depth.

Foraminifers

Rare, moderately well-preserved foraminifers useful for age determinations can be found only in Samples 125-781A-21R-CC, 125-781A-27R-4, 58–60 cm, and 125-781A-27R-CC. The remaining samples are either barren or contain sorted assemblages of undiagnostic juveniles. Sample 125-781A-21R-CC contains a sorted, late Pliocene (Zone N21) foraminiferal assemblage that was determined by the presence of *Globorotalia tosaensis*, *Globorotalia ungulata*, and *Globigerinoides extremus*. Both Samples 125-781A-27R-4, 58–60 cm, and 125-781A-27R-CC are latest late Miocene to early Pliocene (Zones N17b to N19/20, Sample 125-781A-27R-4, 58–60 cm; Zones N17b to N19, 125-781A-27R-CC). The foraminiferal assemblage present in Sample 125-781A-27R-4, 58–60 cm, contains the diagnostic species *Sphaeroidinellopsis praedehiscens*. Sample 125-781A-27R-CC contains a foraminiferal assemblage characterized by *Globigerina nepenthes*, *Globigerinoides bulloides*, and *Sphaeroidinellopsis praedehiscens*. An earliest early Pliocene (Zone N19) age is suspected for Sample 125-781A-27R-CC on the basis of the presence of a form similar to *Globorotalia (H.)* cf. *margaritidae* (first appearance in Zone N19) that, when combined with the presence of *G. bulloides* and *G. nepenthes* (LAD, Zone N19), confines the sample to Zone N19.

Diatoms

Abundant and moderately preserved fragments of *Ethmodiscus rex* are present in Samples 125-781A-1R-CC and 125-781A-15R-CC. A few other diatom species were found in the same two samples. However, we were unable to determine the age of these samples from their diatom content. Traces of poorly preserved *E. rex* also are present in Samples 125-781A-8R-CC and 125-781A-18R-CC.

IGNEOUS AND METAMORPHIC PETROLOGY

Introduction

A basaltic unit (Subunit I) was penetrated in Hole 781A at 67 to 72.2 mbsf. A total of 6.73 m of basaltic rock was then recovered from the next three cores, followed by 10 cores for a total recovery of 23 cm of sediment. Given that the 10 near-empty cores may or may not have contained basaltic material, the thickness of the basaltic unit can be assumed to lie between 12.7 and 25 m. Although the percentage of recovery (28%–55%) of basalt core leaves the possibility of multiple lava flows in this interval, no obvious internal flow boundaries were found in the core. The basaltic unit is directly overlain in Core 125-781A-8R-CC by sediments of late Pliocene biostratigraphic age (CN12b) that show no evidence of thermal baking. The basal contact was not exposed, but the underlying sediments in Section 125-781A-15R-CC also are of late Pliocene age (see "Biostratigraphy" section, this chapter). The basalt unit is of reversed polarity, contrasting with the overlying sediments, which are of normal polarity (see "Paleomagnetism" section, this chapter). The lateral extent of this unit as seen in seismic profiles (see "Underway Geophysics" chapter, this volume), the monotony of the petrography, and the contrast between fresh glass at the top of the unit and altered glass at the base, all suggest that this is a single lava unit. The presence of schlierenlike structures indicates that it is probably a sill. However, dating may be needed to resolve whether it is a submarine lava flow or a sill.

Petrographic description

The basalt is entirely fresh except for the lowermost meter, where glass has been altered to clay. The top of the basalt is an 8-mm-thick chilled margin of vesicle-free, fresh glass having a somewhat lower abundance of phenocrysts (Fig. 4). The proportion of phenocrysts is constant throughout the basalt, but vesicles increase in abundance from 2% to 10% and in size from 1–5 to 8 mm toward the middle part of the unit. In the lowermost part, the vesicles decrease in size (less than 2 mm), but are relatively abundant (10%). Phenocryst-poor, schlierenlike, centimeter-size structures locally occur in the central part of the basalt unit (Fig. 5). Macroscopic observations, augmented by the study of six thin sections representative of the recovered material, show that phenocrysts of plagioclase, olivine, and augite, and glomerocrysts of plagioclase, clinopyroxene, plagioclase + olivine, and plagioclase + clinopyroxene make up 20% to 30% of the rock. Glomerocrysts containing all three phenocryst phases are rare or absent. Some plagioclase phenocrysts contain glass and some contain opaque inclusions. Typical modal proportions, morphology, and size of phenocrysts are from 20% to 25%

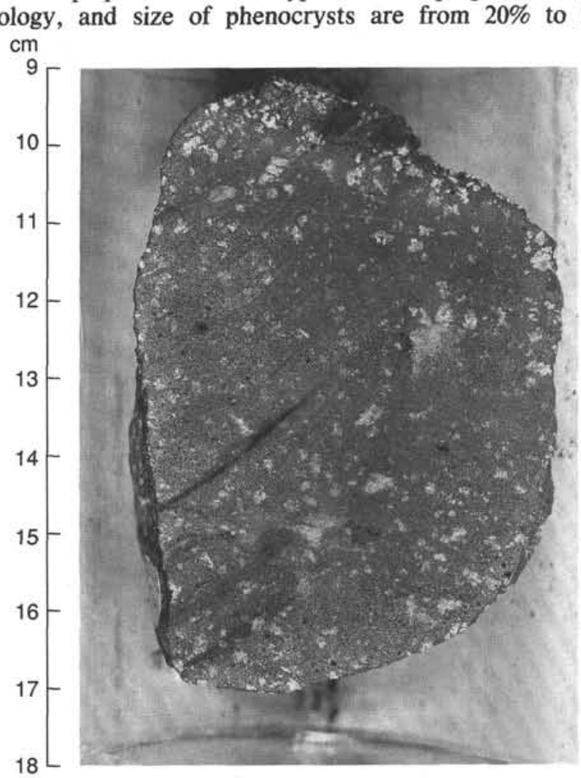

Figure 4. A glassy chilled margin stands out from the rest of a basalt unit by its black color and absence of vesicles (Sample 125-781A-8R-CC, 9–18 cm).

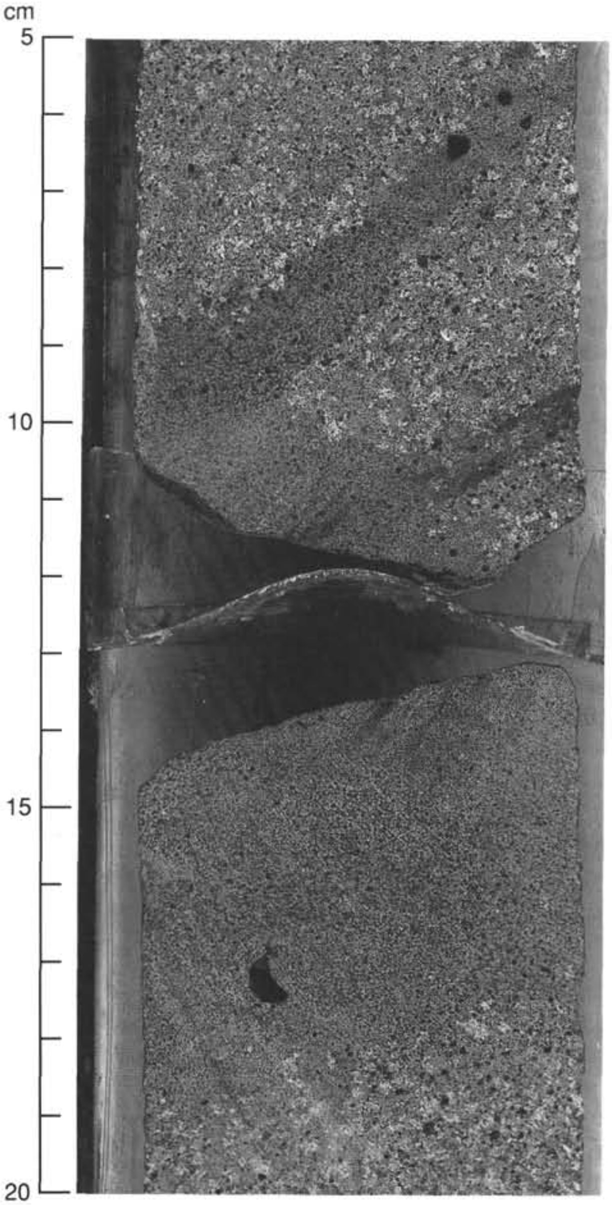

Figure 5. Dark gray structures resembling schlieren from the middle parts of the unit are characterized by the absence of phenocrysts and smaller vesicle size (Sample 125-781A-10R-1, 5–20 cm).

plagioclase (euhedral, less than 3 mm), 1% to 5% olivine (resorbed, round, less than 1 mm), and 1% to 3% clinopyroxene (subhedral to anhedral, 2 mm). Glomerocrysts are commonly smaller than 0.5 mm in size. The groundmass comprises plagioclase (20%–40%), clinopyroxene (10%–25%), olivine (0%–1%), a euhedral opaque phase (possibly magnetite, 5%), and green glass. Proportions of glass vary from up to 80% in the very top to as low as 10% to 15% in the middle of the unit. In the lower parts the glass has been entirely replaced by clay minerals, with the exception of one sample (125-781A-10R-3, 65–67 cm) from the base, which has a low modal proportion (5%) of unaltered glass. Locally, zeolite globules partly fill the vesicles (Fig. 6). The schlierenlike structures are phenocryst-free, have small vesicles (less than 1 mm), and consist of swallowtail and hopper plagioclase (less than 1 mm), feather and radial quench-growth clinopyroxene, and opaque needles in a glassy groundmass.

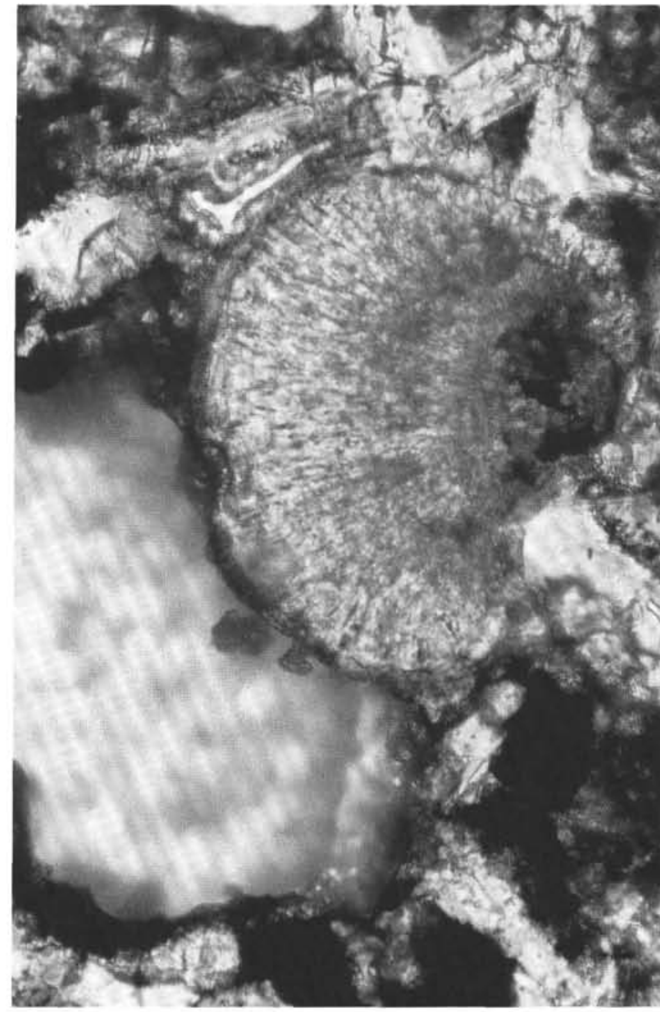

Figure 6. Photomicrograph of a fan-shaped zeolite inclusion in a vesicle (Sample 125-781A-9R-2, 49–51 cm). Field of view is approximately 0.3 mm wide.

IGNEOUS AND METAMORPHIC GEOCHEMISTRY

Drilling in Hole 781 encountered an *in-situ* igneous unit at 67 mbsf. This unit appears to be a single lava flow or sill that is between 12.7 and 25 m thick (28%–55% recovery) and is bound above and below by sediments of late Pliocene age (see "Biostratigraphy" section, this chapter). The unit has a basaltic mineralogy with abundant plagioclase and subordinate clinopyroxene (augite) and olivine phenocrysts in a groundmass dominated by plagioclase, clinopyroxene, olivine, and glass (see "Igneous and Metamorphic Petrology" section, this chapter).

Six samples were analyzed by wavelength spectrometer X-ray fluorescence for abundances of major and trace elements. The samples, originally selected for determining their physical properties, are from Cores 125-781A-8R, 125-781A-9R, and 125-781A-10R. The abundance of each major element was determined from an average of two analyses of a fused glass disk; abundances of trace elements were determined from a pressed powder pellet, using a matrix correction calculated on the basis of the analysis of the fused glass disk (see "Explanatory Notes" chapter, this volume).

Analyses of the major and trace elements are presented in Tables 3 and 4, respectively. Comparison of abundances of trace elements with normal mid-ocean ridge basalt (N-MORB), pre-

Table 3. Abundances of major elements of the six samples taken from the mafic unit in Hole 781A.

Sample no.: Interval (cm):	8R-CC 11–13	9R-1 69–71	9R-2 49–51	10R-1 84–86	10R-2 68–72	10R-3 65–67
SiO_2	48.9	48.42	48.17	48.47	48.66	49.45
TiO_2	0.85	0.86	0.83	0.85	0.84	0.88
Al_2O_3	17.52	17.29	16.98	16.42	17.27	16.97
Fe_2O_3 (Total)	11.86	12.15	11.8	11.87	11.81	12.5
MnO	0.25	0.22	0.24	0.23	0.21	0.24
MgO	4.12	4.3	4.37	4.09	4.38	4.37
CaO	10.96	11.06	10.88	10.52	10.89	10.7
Na_2O	1.77	1.7	1.76	1.79	1.96	1.86
K_2O	0.51	0.41	0.43	0.56	0.38	0.49
P_2O_5	0.06	0.05	0.06	0.06	0.05	0.05
Loss on ignition	0.63	1.26	0.85	1.91	0.74	0.78
Total	98.4	99.01	97.34	98.73	97.94	99.07
Mg#	0.37	0.38	0.39	0.37	0.39	0.38

Note: Elemental analyses (in wt%) were determined on board ship by Don Sims using wavelength-dispersive X-ray fluorescence spectrometry.

sented in Figure 7, was performed with an average of four of the six samples analyzed; the remaining two samples have losses on ignition greater than 1% and thus were excluded on the basis that they may have experienced low-grade alteration.

Major-Element Geochemistry

Little variation in the major elements exists among the samples (Table 3). Silica content varies between 48% and 49%, and magnesium number (i.e., Mg/Mg + Fe) between 0.37 and 0.39, indicating a basaltic composition throughout. The greatest variation is shown by potassium, although this may in part reflect low-grade alteration or mobilization in late-stage magmatic fluids. The low values of potassium and total alkalies suggest that the basalt is a member of the tholeiitic (rather than alkalic or calc-alkaline) rock series. Calcium and aluminium correlate significantly, but vary independently of MgO or SiO_2 (Fig. 8).

Trace-Element Geochemistry

Like the major elements, only minor variations occur in the concentrations of the trace elements (Table 4). These variations may be largely caused by analytical error and minor differences in the proportions of plagioclase phenocrysts. Sample 125-781A-10R-1, 84–86 cm, has the highest concentration of incompatible elements and may be slightly more fractionated than the others. The variation in trace-element abundances relative to N-MORBs is presented here in an

Table 4. Abundances of trace elements of the six samples taken from the mafic unit at Hole 781A.

Sample no.: Interval (cm):	8R-CC 11–13	9R-1 69–71	9R-2 49–51	10R-1 84–86	10R-2 68–72	10R-3 65–67
Nb	0.9	0.9	0.6	1.4	1.0	0.9
Zr	48.4	45.9	46.1	51.9	45.7	48.7
Y	23.2	22.3	22.1	23.8	22.2	22.8
Sr	293.6	293.9	295.2	87.7	293.6	292.6
Rb	6.5	6.4	4.0	13.0	2.4	6.8
Zn	98.0	92.0	71.2	94.0	76.9	81.8
Cu	174.5	183.6	71.8	180.9	141.4	195.6
Ni	7.1	9.0	9.9	11.3	11.0	10.4
Cr	10.8	10.7	10.9	8.3	8.9	11.4
V	407.3	428.2	386.5	353.5	408.0	369.9
Ti	5820.0	5700.0	5400.0	5460.0	5520.0	5340.0
Ce	18.3	31.8	15.0	17.12	6.4	23.1
Ba	169.0	142.2	165.3	157.6	280.2	176.6

Note: Elemental analyses (in ppm) were determined on board ship by Don Sims using wavelength-dispersive X-ray fluorescence spectrometry.

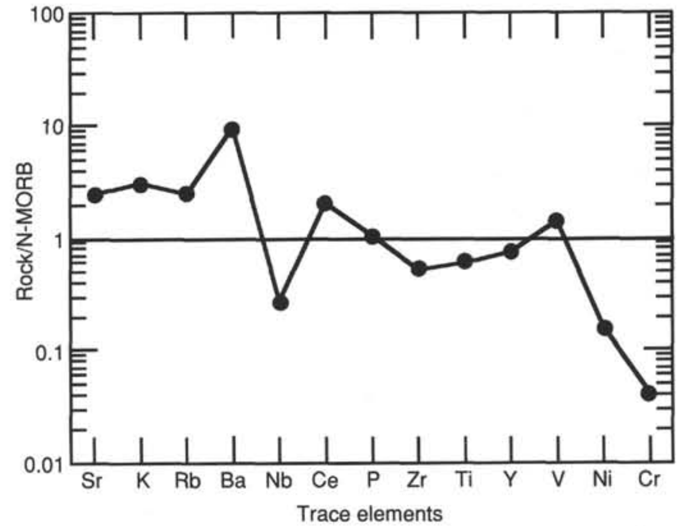

Figure 7. An average of four samples from the mafic unit, normalized to N-MORB, showing relative enrichment in the large-ion-lithophile and light rare earth elements and depletion in the high-field-strength and compatible elements.

N-MORB normalized multi-element diagram (Fig. 7). The compatible trace elements, nickel and chromium, as well as the high-field-strength (HFS) elements, titanium, zirconium, yttrium, and niobium, are depleted relative to N-MORBs. However, the large-ion-lithophile (LIL) elements, strontium, rubidium, potassium, barium, and cerium, a light rare earth element, are enriched with respect to N-MORBs.

Petrogenesis and Eruptive Setting

The petrology of the mafic unit indicates that plagioclase, clinopyroxene, and olivine were the main crystallizing phases (see "Igneous and Metamorphic Petrology" section, this chapter). The co-variation of Al_2O_3 and CaO and the inverse relationship of strontium with the incompatible trace elements may be attributed to either plagioclase fractionation or variation in the proportion of plagioclase phenocrysts. Overall, however, the small variation between samples in the abundances of major and trace elements is consistent with the hypothesis of only a single lava flow or sill that underwent little internal fractionation.

The enrichment of the mafic unit in LIL elements and the depletion in HFS elements, especially niobium, relative to N-MORBs is characteristic of a subduction-related environment of genesis. In such environments the LIL elements are selectively introduced into the mantle wedge during dewatering, and perhaps partial melting, of the subducted oceanic slab. This is supported by the similar abundance of chromium and yttrium in the mafic unit relative to island-arc tholeiites (IAT), compared with MORBs or boninites (Fig. 9). The trace-element data provide evidence of a two-component petrogenetic model for the mafic unit: an addition of LIL elements relative to N-MORBs, indicative of a subduction component, and a lower abundance of HFS elements relative to N-MORBs, indicative of derivation from a depleted or less-fertile source than that for N-MORBs or at a greater degree or partial melting. Therefore, on the basis of shipboard geochemistry, the mafic unit encountered in Hole 781A can be categorized as a basalt of the island-arc-tholeiite series, an interpretation that is consistent with an origin within the mantle wedge above the subducting Pacific Plate.

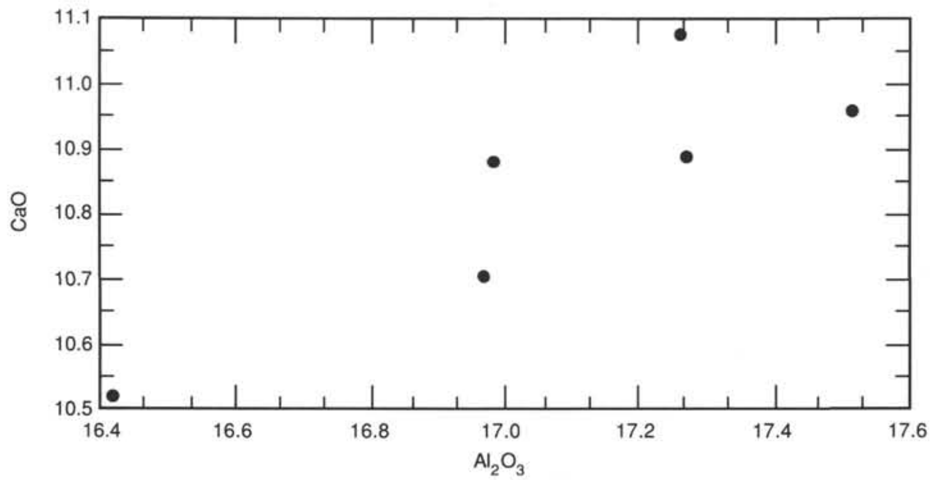

Figure 8. Proportional co-variation of CaO with Al_2O_3 (in wt%) may reflect addition or loss of plagioclase phenocrysts.

SEDIMENT/FLUID GEOCHEMISTRY

Sediment Geochemistry

Cores from Site 781 were analyzed on board ship for inorganic carbon and for total carbon, nitrogen, and sulfur using the techniques described in the "Explanatory Notes" chapter (this volume). The organic carbon content was then calculated by difference. These results are presented in Table 5 and in Figure 10. The sediments at Site 781 are considerably richer in $CaCO_3$ and organic carbon, and poorer in nitrogen and sulfur, than those at Sites 778, 779, and 780 on Conical Seamount. The $CaCO_3$ content varies from 0.2 to 8.6 wt%, with most values between 2 and 5 wt%. The lowest values occur between 49 and 65 mbsf, whereas the highest values are near the bottom of Hole 781A, at 227 and 255 mbsf. The organic carbon content increases from 0.26 wt% near the seafloor to a maximum value of 1.31 wt% at 65 mbsf. Most values fall between 0.6 and 0.8 wt%. Nitrogen was detected in only one sample, at a concentration of 0.12 wt% at 0.73 mbsf. Sulfur was not detected in any of the samples and therefore is uniformly less than 0.06 wt%.

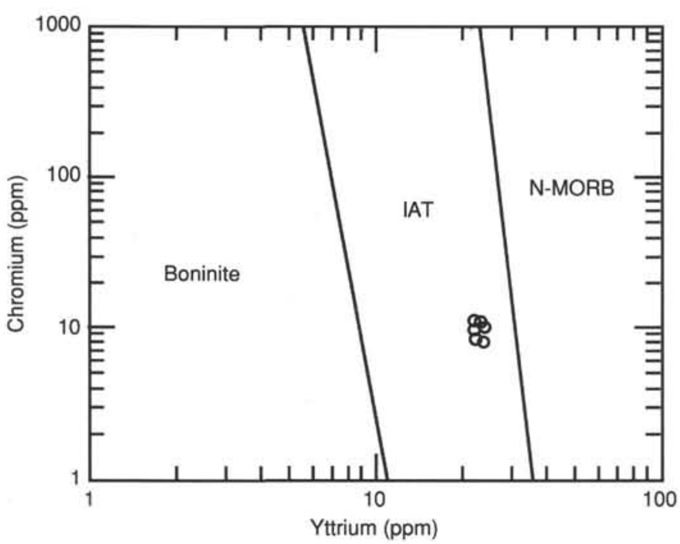

Figure 9. This diagram in chromium/yttrium space (after Pearce and Wanming, 1988) discriminates among environments of formation for boninite, island-arc tholeiite (IAT), and normal mid-ocean ridge basalt (N-MORB). Samples from the mafic unit plot within the field for island-arc tholeiites.

Fluid Geochemistry

The concentration of methane measured for 5-cm^3 sediment headspace samples is uniformly low, usually less than 20 mL/L (Table 6). Methane was the only hydrocarbon detected. These values are even lower than those at Site 778, and they are much lower than those at Sites 779 and 780.

Compared with interstitial waters at Sites 778, 779, and 780, the waters squeezed from sediments at Site 781 (Table 7) are much more like waters from typical deep-sea sediments. The Ph is much lower and in the normal range of 7.5 to 8.5 (Fig. 11). Alkalinity increases slightly from the seawater value

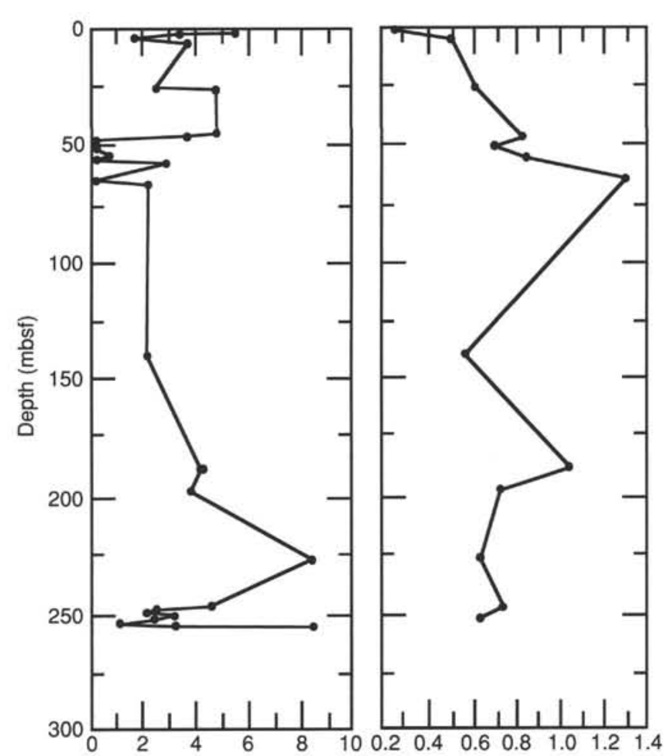

Figure 10. Abundances of calcium carbonate and total organic carbon (in wt%) in sediments from Site 781.

Table 5. Total nitrogen, sulfur, and carbon; organic carbon; and carbonate carbon in sediments of Hole 781A.

Core, section, interval (cm)	Depth (mbsf)	Total N (wt%)	Total sulfur (wt%)	Total carbon (wt%)	Inorganic carbon (wt%)	Organic carbon (wt%)	$CaCO_3$ (wt%)
125-781A-1R-1, 73–75	0.73	0.12	nd	0.86	0.60	0.26	5.0
1R-2, 69–71	1.52				0.21		1.7
1R-3, 19–21	2.52				0.41		3.4
1R-5, 87–89	6.20	nd	nd	0.96	0.44	0.52	3.7
4R-1, 54–56	26.44	nd	nd	0.93	0.30	0.63	2.5
4R-CC, 6–8	26.63				0.58		4.8
6R-1, 64–66	45.54				0.58		4.8
6R-2, 64–66	47.04	nd	nd	1.29	0.45	0.84	3.7
6R-3, 64–66	48.54				0.03		0.2
6R-4, 64–66	50.04				0.03		0.2
6R-5, 15–16	51.05				0.02		0.2
6R-6, 10–12	51.50	nd	nd	0.74	0.02	0.72	0.2
6R-CC, 4–6	51.67				0.02		0.2
7R-1, 38–40	54.88				0.08		0.7
7R-2, 38–40	56.38	nd	nd	0.88	0.02	0.86	0.2
7R-3, 38–40	57.88				0.35		2.9
8R-1, 85–87	65.35	nd	nd	1.34	0.03	1.31	0.2
8R-2, 72–74	66.72				0.27		2.2
16R-CC, 7–9	140.07	nd	nd	0.86	0.27	0.59	2.2
21R-1, 8–10	188.28	nd	nd	1.58	0.52	1.06	4.3
21R-CC, 14–16	188.56				0.51		4.2
22R-CC, 7–9	197.97	nd	nd	1.22	0.47	0.75	3.9
25R-CC, 11–13	227.01	nd	nd	1.68	1.02	0.66	8.5
27R-1, 21–23	246.21				0.56		4.7
27R-2, 21–23	247.71	nd	nd	1.07	0.31	0.76	2.6
27R-3, 21–23	249.21				0.27		2.2
27R-4, 21–23	250.71				0.40		3.3
27R-5, 21–23	252.21	nd	nd	0.96	0.30	0.66	2.5
27R-6, 21–23	253.71				0.15		1.2
27R-7, 3–5	255.03				0.40		3.3
27R-CC, 13–15	255.35				1.03		8.6

nd = not detected.

to 3.1 at 57 mbsf and then decreases to 0.7 at 237 mbsf near the bottom of Hole 781A. Ammonia increases with depth at about the same rate as at Site 778, reaching a maximum value of 197 mmol/kg near the bottom of Hole 781A. Silica is much higher than in waters from Conical Seamount, ranging from 260 to 630 mmol/kg. Sulfate is largely unchanged at the seawater value. Magnesium decreases to about one-half the seawater value with depth, whereas calcium, sodium, and potassium all increase (Fig. 12). Chlorinity and salinity also increase with depth, by less than 2% (Fig. 13).

The slight increase in alkalinity in the upper 60 m of sediment may result from oxidation of organic matter by bacteria that also reduce seawater sulfate. The increase in ammonia may result from the same process. The changes in magnesium, calcium, and sodium may be caused by reaction with volcanic matter in the sediments or in the underlying basement rocks; on the basis of the large changes with depth, the latter reason is more likely. The small increases in chlorinity and salinity with depth were probably caused by the increased salinity of ocean bottomwater during the Pleistocene glaciations (McDuff, 1985).

Table 6. Results of headspace-gas analyses of sediments from Hole 781A.

Core, section, interval (cm)	Depth (mbsf)	Methane (μL/L)[a]	Methane (μM)[b]
125-781A-1R-2, 135–140	2.88	11	0.9
4R-1, 60–62	26.51	19	1.7
6R-4, 135–140	50.7	81	41.2
7R-2, 135–140	57.3	81	51.3
8R-2, 0–3	66.02	11	1.0
22R-CC, 12–15	198.03	12	1.1
24R-CC, 11–14	227.03	12	1.1
26R-1, 29–32	236.81	11	1.0
27R-4, 137–140	251.89	3	0.2

[a] Microliters of gas per liter of wet sediment.
[b] Micromoles of methane per liter of interstitial water, assuming a porosity of 50%.

PALEOMAGNETISM

Magnetic Remanence

Although the recovery from Hole 781A was poor (16%), combined paleomagnetic and biostratigraphic data (see "Biostratigraphy" section, this chapter) have enabled us to construct a tentative magnetostratigraphy for the sediments in the upper 70 m of this hole. The natural remanent magnetization (NRM) of the archive halves of Cores 125-781A-1R, 125-781A-6R to 125-781A-10R, 125-781A-21R, and 125-781A-27R was measured using the cryogenic magnetometer. Intensities decreased systematically downhole from 1000 to 100 mA/m between the top of Section 125-781A-6R-1 and the base of Section 125-781A-1R-2, and also decreased from 600 to 10 mA/m between the top of Section 125-781A-8R-1 and the base of Section 125-781A-8R-CC. A systematic increase in intensity (from about 100 to 1500 mA/m) was observed between the top of Section 125-781A-27R and 35 cm below the top of Section 125-781A-27R-5.

Sections were then alternating-field (AF) demagnetized at 5 and 10 mT and measured between successive steps. Demagnetization typically reduced the intensity by about 20% to 35% of the NRM value. Changes in the declination and inclination were generally between 10° and 20°, making polarity evaluations somewhat difficult. Those intervals within Hole 781A to which we felt confident in assigning a polarity are summarized in Table 8.

Table 7. Composition of interstitial waters from sediments in Hole 781A.

Sample no.	Core, section, interval (cm)	Vol. (mL)	Squeeze T (°C)	Depth (mbsf)	pH	Salinity (R.I.,%)	Salinity (calc.,%)	Chlorinity (mmol/kg)	Alkalinity (meq/kg)	Sulfate (mmol/kg)	Sodium (mmol/kg)	Potassium (mmol/kg)
Surface seawater (4 March 1989)					8.10	35.5	34.85	542.6	2.386	27.98	464.8	10.05
IW-1	125-781A-1R-2, 140–150	58	3	2.95	7.97	35.2	35.15	548.9	3.266	26.60	469.8	10.42
IW-2	4R-1, 62–67	20	3	26.55	8.00	34.8	35.44	551.3	2.487	27.97	473.1	11.61
IW-3	6R-1, 140–150	35	3	46.35	8.00	35.5	35.75	555.2	2.877	28.34	478.2	10.76
IW-4	6R-4, 140–150	44	3	50.85	8.09	36.5	35.63	556.2	2.904	26.73	478.6	11.81
IW-5	7R-2, 140–150	58	3	57.45	8.34	37.0	35.99	559.1	3.016	28.04	482.7	11.71
IW-6	8R-2, 103–113	60	3	67.08	8.51	35.5	35.60	551.3	2.793	28.77	477.5	11.57
IW-7	21R-CC, 30–36	27	3	197.57	8.34	36.0	36.19	556.2	1.339	29.92	490.1	7.04
IW-8	26R-1, 32–42	19	3	236.87	8.07	36.5	35.84	560.2	0.688	25.77	482.9	5.92

Values absent from table were not determined.

Discrete specimens were taken from the working halves of Cores 125-781A-1R, 125-781A-6R to 125-781A-10R, 125-781A-21R, 125-781A-24R, 125-781A–26R, and 125-781A-27R for additional analysis. These specimens were processed through fields of 0, 5, 10, and 15 mT using the cryogenic magnetometer. Results from these specimens are summarized in Table 9. Data from Cores 125-781A-21R to 125-781A-27R are included, although the relatively disturbed material at these levels (probably resulting from drilling) renders any polarity evaluation suspect.

In most cases, each specimen records a similar polarity to the relevant interval in the archive half of the core. It must be noted, however, that specimens taken from Sections 125-781A-6R-2 and 125-781A-6R-3 are of opposite polarity to the same level within the archive-half of the core (normal polarity instead of reversed). Polarity for these levels should

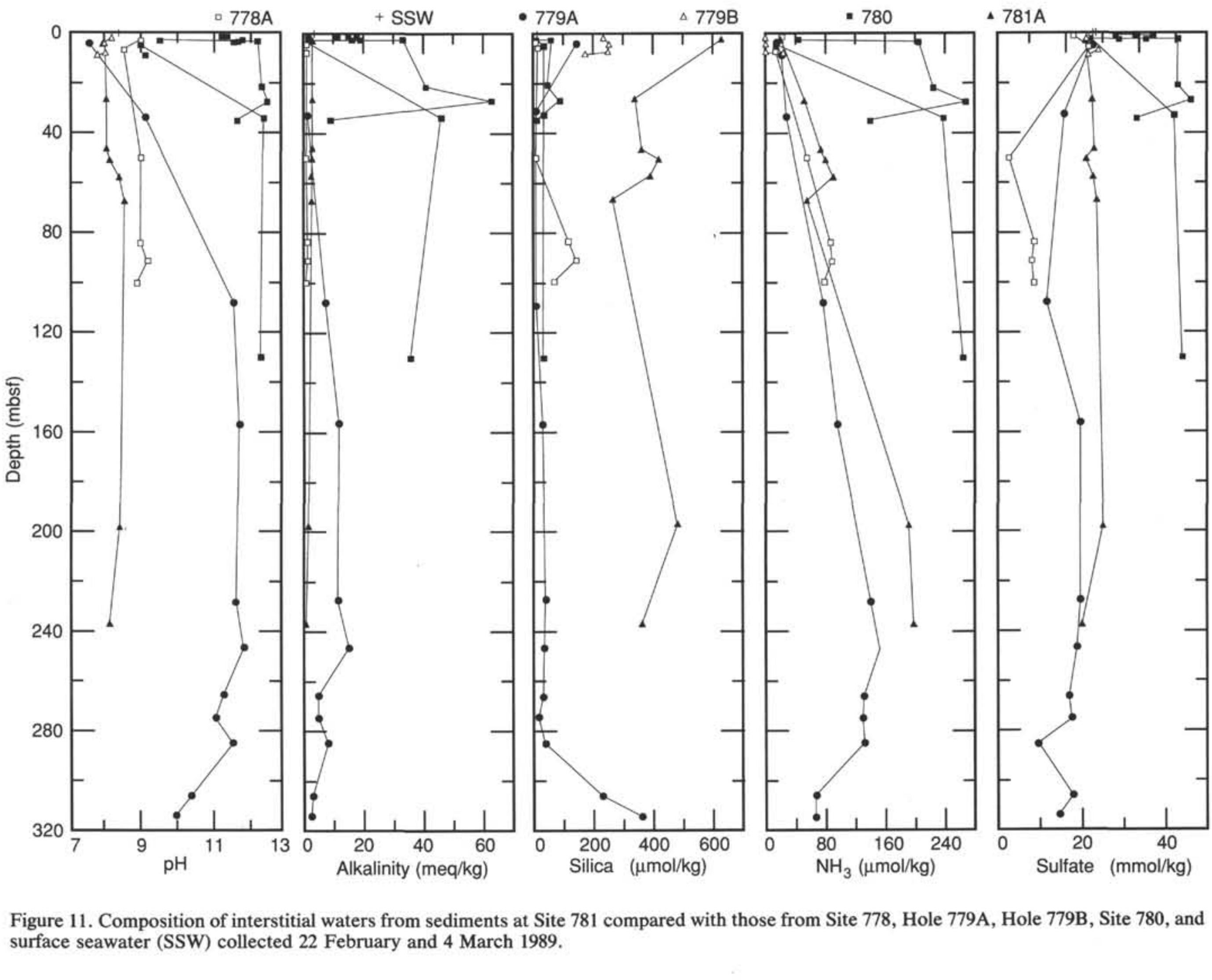

Figure 11. Composition of interstitial waters from sediments at Site 781 compared with those from Site 778, Hole 779A, Hole 779B, Site 780, and surface seawater (SSW) collected 22 February and 4 March 1989.

Table 7 (continued).

Calcium (mmol/kg)	Magnesium (mmol/kg)	Bromide (mmol/kg)	Silica (μmol/kg)	Ammonia (μmol/kg)	Phosphate (μmol/kg)
10.17	52.89	0.85	5	<5	
10.34	52.24	0.80	628	23	
11.04	51.46	0.83	338	51	8.42
12.27	50.62	0.73	361	72	2.91
12.09	48.99	0.89	421	80	0.91
12.60	49.26	0.70	391	90	1.45
11.10	50.21	0.71	264	55	1.02
29.69	30.44	0.77	480	192	0.27
37.63	24.14	0.84	361	197	

be based on whole-core data, but further sampling and shorebased analyses of this interval will be required before this correlation can be established.

Recovery in Cores 125-781A-8R (very base), 125-781A-9R, and 125-781A-10R was about 6.5 m of basalt from either a sill or a flow having an estimated total thickness of between 12.7 and 25 m (see "Igneous and Metamorphic Petrology" section, this chapter). This body is defined as a single subunit (IC) in the "Lithostratigraphy" section (this chapter) and has a reversed polarity. The next datable horizon beneath this subunit is found in Core 125-781A-15R, where sediments have been assigned to Okada and Bukry's (1980) nannoplankton Zone CN12b. Core 125-781A-8R, immediately above the sill, has a normal magnetic polarity and contains nannoplankton that have been assigned to Zone CN12b. According to data presented by Berggren et al. (1985), the nannoplankton Zones CN12a/CN12b are associated with the Gauss Normal Polarity Chron. If this igneous body is a flow, then it must pre-date the sediments immediately overlying it. Its reversed polarity magnetization would then be a record of one of the short reversed events within the Gauss Normal Polarity Chron. Alternatively, if the igneous body is a sill, then it must post-date the normally magnetized sediments in Core 125-781A-8R. In that case, its magnetization could have been acquired anytime during the Matuyama Reversed Polarity Chron (0.73 to 2.47 Ma).This flow vs. sill argument can only be properly re-solved by radiometric dating and detailed petrofabric studies.

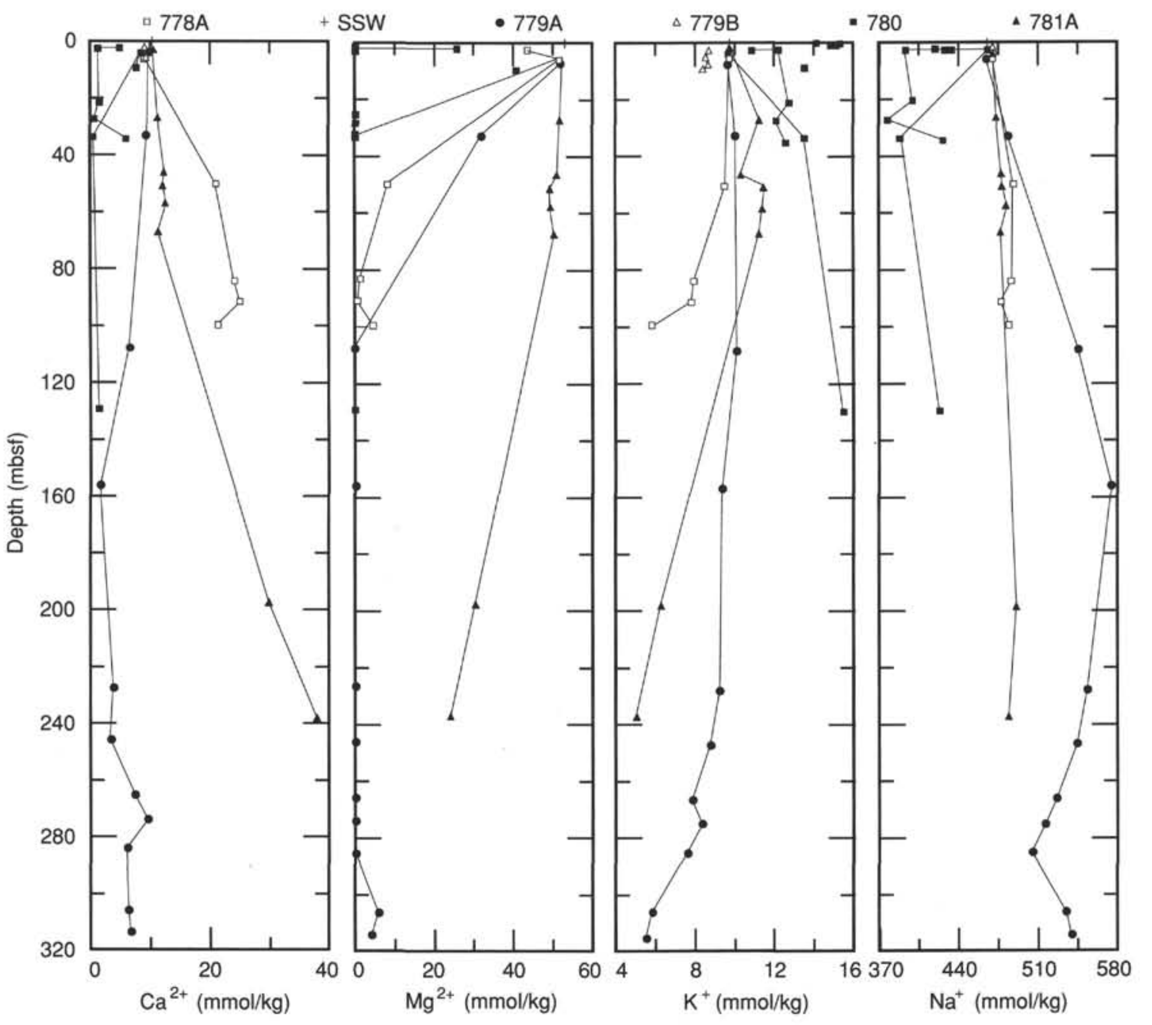

Figure 12. Composition of interstitial waters from sediments at Site 781 compared with those from Site 778, Hole 779A, Hole 779B, Site 780, and surface seawater (SSW) collected 22 February and 4 March 1989.

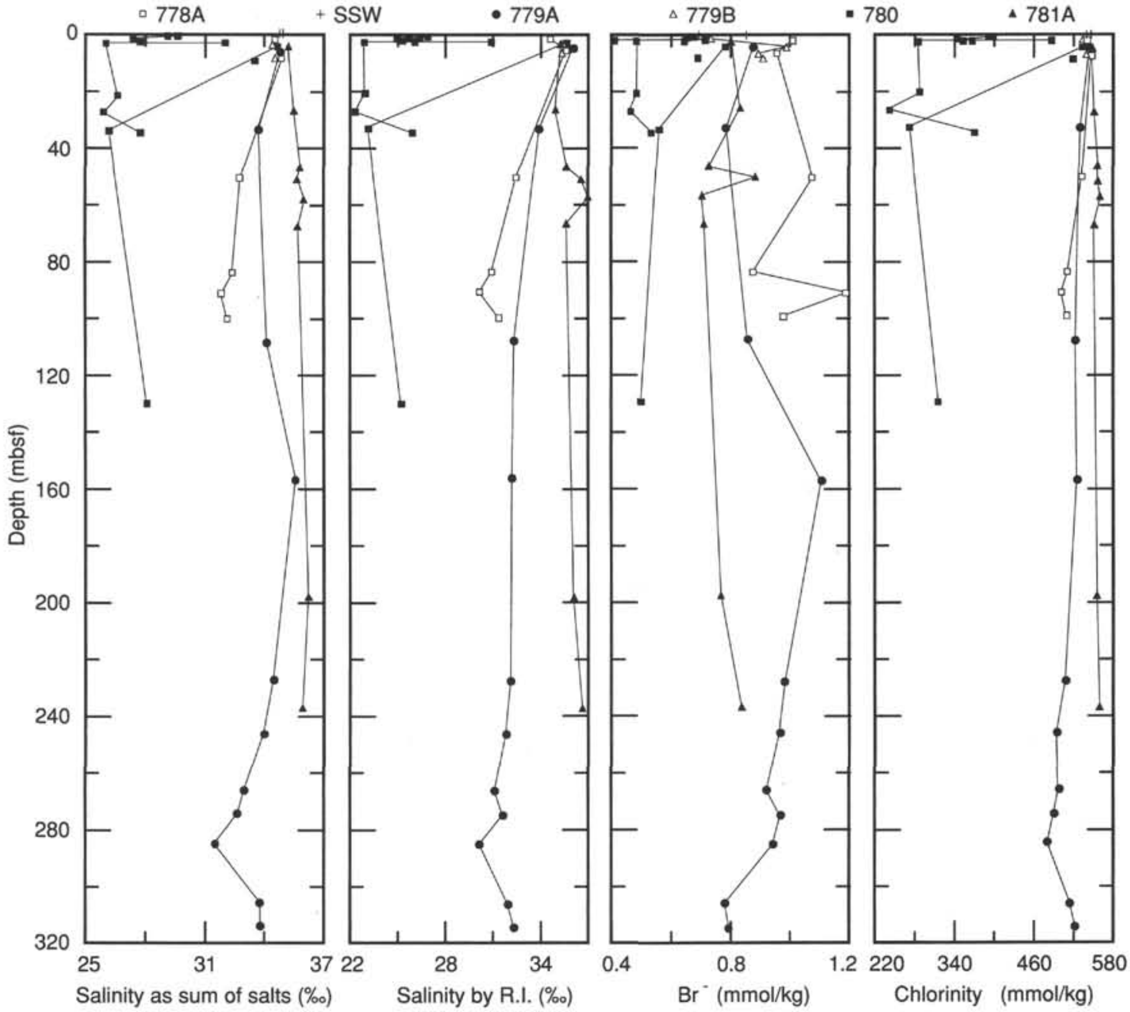

Figure 13. Composition of interstitial waters from sediments at Site 781 compared with those from Site 778, Hole 779A, Hole 779B, Site 780, and surface seawater (SSW) collected 22 February and 4 March 1989.

Magnetic Susceptibility

Whole-core magnetic susceptibilities were measured using the multisensor track. In Cores 125-781A-1R through 125-781A-10R, the susceptibilities range from 0 to 8×10^{-3} SI. There is no marked difference in susceptibility between the igneous body and the overlying sediments. However, a huge increase in susceptibility is observed within Core 125-781A-27R. The value increases from 6×10^{-3} SI at 247 msbf to 40×10^{-3} SI at 254 mbsf (Fig. 14). A similar increase is present in the GRAPE density data (see "Physical Properties" section, this chapter, Fig. 18). Figure 15 is a plot of susceptibility vs.

Table 8. Specific intervals in Hole 781A to which magnetic polarity was assigned.

Core, section, interval	Polarity	Nannofossil zone	Age	Magnetochron
125-781-1R-2, 0–115 cm	N	CN/15	late Pleistocene	Bruhnes
125-781-1R-5, 75–147 cm	N	CN/15	late Pleistocene	Bruhnes
125-781-6R-2, 30 cm to (upper) 125-781-6R-3, 140 cm	R	CN14a	early Pleistocene	Matuyama
125-781-6R-6, 0 cm to (upper) 125-781-6R, CC, 18 cm	R	CN14a	early Pleistocene	Matuyama
125-781-7R-1, 0 cm to (upper) 125-781-7R, CC, 21 cm	R	CN14a	early Pleistocene	Matuyama
125-781-8R-1, 0 cm to 125-781-8R-2, 113 cm	N	CN12b	late Pleistocene	Gauss
125-781-9R-1, 0 cm to 125-781-9R-3, 150 cm	R		(?)	
125-781-10R-1, 0 cm to 125-781-10R-3, 113 cm	R		(?)	

Note: Core 125-781A-15R is the youngest biostratigraphically dated level below 125-781A-10R and has been assigned to CN12b.

Table 9. Paleomagnetic data for discrete specimens taken from Hole 781A.

Section	Top (cm)	NRM DEC	NRM INC	NRM INT	RM at 15mT DEC	RM at 15mT INC	RM at 15mT INT	Polarity
125-781A-1R-2	83	59.3	32.9	91.6	57.2	32.6	69.8	N
125-781A-1R-3	36	105.8	6.8	65.2	101.0	3.6	43.9	?
125-781A-1R-4	74	162.8	31.1	107.0	162.0	31.4	74.6	N
125-781A-1R-5	116	157.8	−2.0	120.0	159.0	−4.6	90.6	?
125-781A-6R-1	94	89.7	24.8	33.4	87.9	18.8	22.6	N
125-781A-6R-2	94	232.6	5.0	8.8	87.9	23.6	2.4	N
125-781A-6R-3	94	8.8	39.2	40.6	24.4	33.8	34.2	N
125-781A-6R-4	94	218.8	12.0	6.5	244.5	−6.4	3.3	R
125-781A-6R-5	13	312.3	−17.8	29.3	308.4	−14.8	36.8	R
125-781A-7R-1	50	158.7	−65.0	127.0	161.9	−68.5	129.0	R
125-781A-7R-2	50	20.5	−0.4	30.5	27.2	−13.0	34.5	R
125-781A-7R-3	50	301.7	9.2	58.4	305.1	4.0	55.6	R
125-781A-8R-1	121	1.0	44.5	160.0	1.2	43.9	115.0	N
125-781A-8R-2	32	25.3	37.7	40.8	21.3	31.6	26.3	N
125-781A-9R-1	58	314.5	−25.1	1770.0	309.3	−23.2	1040.0	R
125-781A-9R-2	38	43.1	18.8	1620.0	46.1	2.2	1020.0	R
125-781A-9R-3	44	253.2	19.4	1420.0	262.3	4.0	583.0	R
125-781A-10R-1	23	137.5	−17.6	1740.0	145.7	−11.0	1120.0	R
125-781A-10R-2	105	207.6	−5.4	850.0	201.2	−5.8	209.0	R
125-781A-10R-3	13	85.2	12.0	347.0	88.0	6.4	54.5	R
125-781A-21R-1	16	205.1	18.0	23.6	210.8	14.7	15.1	N
125-781A-21R-C	19	352.4	−26.3	43.5	354.5	−25.6	27.2	R
125-781A-24R-C	26	297.2	−15.0	461.0	298.4	−10.8	275.0	R
125-781A-26R-C	8	73.8	20.4	24.2	65.9	5.5	24.3	R
125-781A-27R-2	120	36.9	11.0	152.0	37.0	−12.9	59.9	R
125-781A-27R-3	38	347.0	32.4	248.0	55.4	24.1	188.0	N
125-781A-27R-4	83	70.2	14.0	417.0	8.2	14.8	183.0	N
125-781A-27R-5	146	147.6	53.5	716.0	148.5	73.0	144.0	N
125-781A-27R-6	58	161.0	51.7	579.0	332.0	73.0	132.0	N
125-781A-27R-7	15	312.6	10.9	118.0	312.6	14.4	91.0	N
125-781A-27R-C	4	135.0	−28.8	803.0	133.8	−16.0	463.0	R

NRM = Natural remanent magnetization; RM = Remanence after demagnetization; DEC = Declination (degrees); INC = Inclination (degrees); INT = Intensity (mA/m); Top = distance from the top of the section. The specimens from Sections 125-781A-21R through 125-781A-27R are from intervals where it was impossible to work out the magnetostratigraphy for the whole-core archive sections.

bulk density for Core 125-781A-27R (between 246 and 256 mbsf). One can see very good correlation of these two parameters, with a correlation coefficient of 0.935. Detailed examination of this core revealed macroscopic pieces of metal (up to 2 mm in diameter), indicating that the correlation between susceptibility and density is almost certainly a result of contamination of the sediment by material from the drilling assembly. This suggests that the core was greatly disturbed by drilling, as contaminants were found in the center of the core, and that the material recovered from between 246 and 256 mbsf contains drill cuttings and does not reflect the stratigraphy at the bottom of Hole 781A.

PHYSICAL PROPERTIES

Thermal conductivity, bulk density, compressional-wave velocities, index properties (bulk and grain densities, porosity, water content, and void ratio), magnetic susceptibility, and shear strength were measured in rocks from Site 781 (Tables 10 and 11). Magnetic-susceptibility data are discussed in the "Paleomagnetism" section (this chapter). Poor recovery from depths of 70 to 220 mbsf prevented most physical properties from being measured in this interval.

Measurements of thermal conductivity for soft rocks from Hole 781A were uniformly low, with no values greater than 1.1 W/mK (Table 11). Thermal conductivity in these samples does not vary with depth in the hole (Fig. 16). Thermal conductivities measured in the basalt are also low (0.556 to 0.885 W/Mk) and, again, no correlations with depth are observed.

Bulk densities were determined from the GRAPE sensor on the multisensor track (MST). The data show considerable scatter, most commonly related to small voids in the sections. However, an increase in average bulk density with increasing depth (Fig. 17) is apparent. GRAPE densities from the lowest intervals of Core 125-781A-27R show a large density increase from 1.8 to 2.0 g/cm^3 (Fig. 18). A similar pattern of increase is seen in magnetic-susceptibility data from the same sections. These patterns may be related to the increased abundance of igneous rock fragments in drill cuttings and iron filings from the drill assembly at the bottom of the hole, and not to geologic processes (see discussion in "Paleomagnetism" section, this chapter).

Index properties measured were the wet weight, dry weight, and dry volume of discrete samples. From these data, wet volume, bulk density, grain density, water content, porosity, and void ratio were calculated. These data are presented in Table 9. Bulk densities of sediment samples ranged from 1.51 to 2.06 g/cm^3, and grain densities had a range of 2.4 to 2.8 g/cm^3. Porosities in the sediment samples ranged from 41% to 74%. The variation of index properties with depth is shown in Figure 19. No significant correlations with depth were observed.

The compressional-wave velocity logger on the MST was successful in obtaining data from many of the sections recovered at Site 781; however, poor coupling of the transducers remained a problem, preventing complete logging of some of these recovered sections. The velocity data show considerable scatter (1400 to 2100 m/s), which probably is related to voids in the cores. Nonetheless, compressional-wave velocities increased with depth (Fig. 20).

Compressional-wave velocities in hard-rock samples were measured on the Hamilton frame apparatus in orthogonal

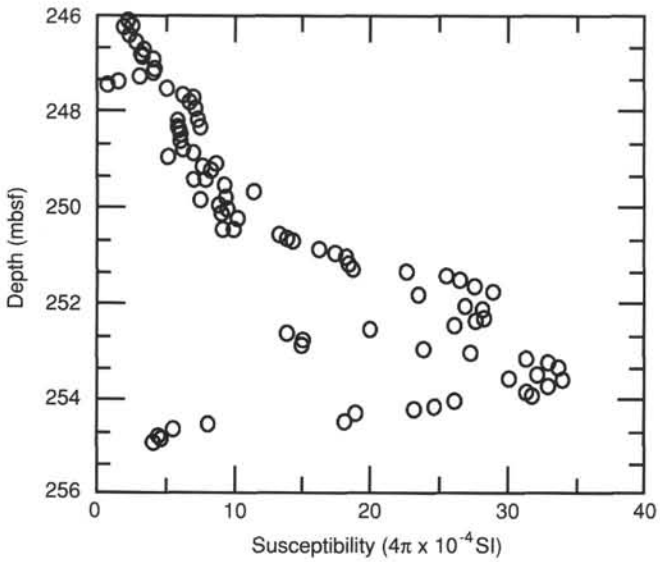

Figure 14. Plot of downhole variations in susceptibility for Core 125-781A-27R.

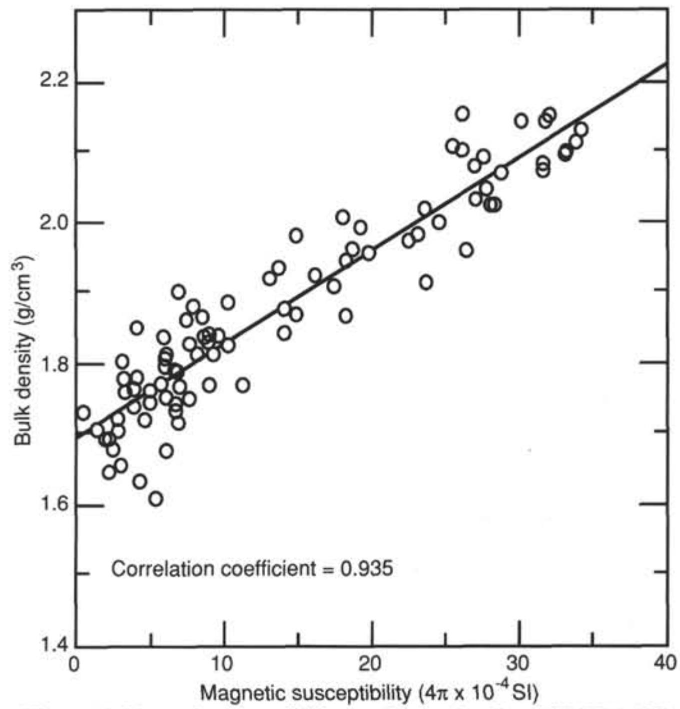

Figure 15. Magnetic susceptibility vs. density for Core 125-781A-27R.

directions (Table 10). The reported velocities are low for basalts and range from 3906 to 5300 m/s: these values reflect the strong effect of fractures and microcracks on compressional-wave velocities at low confining pressures. The measurement of velocities in two directions allows for an initial assessment of the seismic anisotropy of the rock. Velocities measured along the length of the core range from 4140 to 5270 m/s, and those measured perpendicular to the core axis range from 3960 to 5180 m/s. Therefore, these samples are not seismically anisotropic at low confining pressures.

Table 10. Index-property data for Hole 781A.

Core, section, interval (cm)	Depth (mbsf)	Bulk density (g/cm^3)	Grain density (g/cm^3)	Porosity (%)	Water content (%)	Void ratio
125-781A-1R-1, 73–75	0.73	1.53	2.6	72.9	50.7	0.73
1R-2, 69–71	1.52	1.55	2.5	74.2	51.0	0.74
1R-3, 19–21	2.52	1.58	2.48	64.4	43.4	0.64
1R-5, 87–89	6.2	1.64	2.57	67.5	43.8	0.68
4R-1, 54–56	26.44	1.59	2.6	66.4	44.3	0.66
4R-CC, 13–6	26.63	1.64	2.62	64.9	42.0	0.65
6R-1, 64–66	45.54	1.62	2.43	64.8	42.6	0.65
6R-2, 64–66	47.04	1.65	2.6	65.7	42.2	0.66
6R-3, 64–66	48.54	1.52	2.67	70.9	49.6	0.71
6R-4, 64–66	50.04	1.51	2.79	74.6	52.6	0.75
6R-5, 15–16	51.05	1.51	2.9	72.3	51.0	0.72
6R-CC, 13–4	51.67	1.51	2.67	72.4	50.8	0.72
7R-1, 38–40	54.88	1.65	2.72	65.4	42.1	0.65
7R-2, 38–40	56.38	1.52	2.36	65.0	45.4	0.65
7R-3, 38–40	57.88	1.63	2.62	65.4	42.6	0.65
8R-1, 85–87	65.35	1.51	2.68	71.8	50.6	0.72
8R-2, 72–74	66.72	1.69	2.71	63.6	40.1	0.64
8R-CC, 13–11	67.24	2.65	2.76	6.4	2.5	0.06
9R-1, 69–71	73.29	2.63	2.73	6.0	2.4	0.06
9R-2, 49–51	74.47	2.59	2.75	8.9	3.6	0.09
9R-3, 111–113	76.43	2.60	2.69	2.1	0.8	0.02
10R-1, 84–86	83.14	2.62	2.69	4.0	1.6	0.04
10R-2, 68–70	84.43	2.61	2.71	5.5	2.2	0.05
10R-3, 65–70	85.76	2.62	2.72	6.3	2.6	0.06
16R-CC, 13–7	140.07	1.71	2.72	48.7	30.2	0.49
21R-CC, 14–16	188.56	1.61	2.57	62.7	41.3	0.63
22R-CC, 13–7	197.97	1.55	2.42	63.0	43.3	0.63
25R-CC, 13–11	227.01	1.64	2.54	60.7	39.3	0.61
27R-1, 21–23	246.21	1.67	2.64	60.8	38.7	0.61
27R-2, 21–23	247.71	1.66	2.5	57.4	36.7	0.57
27R-3, 21–23	249.21	1.79	2.62	52.4	31.1	0.52
27R-4, 21–23	250.71	1.79	2.71	55.1	32.7	0.55
27R-5, 21–23	252.21	1.76	2.75	57.8	34.9	0.58
27R-6, 21–23	253.71	2.06	2.78	41.0	21.1	0.41
27R-CC, 13–15	255.35	1.71	2.71	59.8	37.1	0.60

Table 11. Physical-property data for Hole 781A.

Core, section, interval (cm)	Depth (mbsf)	Thermal conductivity (W/mK)	Ultimate strength (kPa)	"A" velocity (km/s)	"B" velocity (km/s)
125-781A-1R-2, 43	1.26	0.824			
1R-2, 91–92	1.81		8.1		
1R-2, 125–126	2.15		12.8		
1R-3, 22	2.55	0.924			
1R-3, 32–33	2.72		7.5		
1R-5, 97	6.3	0.184			
4R-1, 26	26.16	0.946			
4R-CC, 4	26.61	1.008			
6R-1, 89	45.79	0.403			
6R-3, 18–19	48.19		8.7		
6R-3, 89	48.79	0.911			
6R-3, 123–124	49.24		35.9		
6R-4, 78–79	50.29		116.1		
6R-4, 89	50.34	0.935			
6R-4, 118–119	50.75		75.3		
6R-5, 17	51.07	1.023			
6R-5, 20–21	51.1		33.9		
6R-6, 17	51.57	0.934			
7R-1, 68	55.18	0.967			
7R-2, 68	56.68	0.866			
7R-3, 68	58.18	0.929			
8R-1, 79	65.29	0.94			
8R-2, 39	66.39	1.058		4.74	4.72
9R-1, 68	73.28	0.602		4.14	3.96
9R-2, 47	74.45	0.677		4.82	4.84
9R-3, 100	76.32	0.677		4.6	4.4
10R-1, 73	83.03	0.885		5.27	5.18
10R-2, 60	84.35	0.556		5.16	4.9
10R-3, 60	85.71	0.588		5.07	5.1
21R-1, 11	188.31	0.577			
26R-1, 14	236.64	0.997			
27R-1, 60	246.6	0.691			
27R-2, 70	248.2	0.854			
27R-3, 78	249.78	1.063			
27R-4, 72	251.22	1.02			
27R-5, 66	252.66	0.095			
27R-6, 71	254.21	1.054			
27R-7, 10	255.1	0.949			

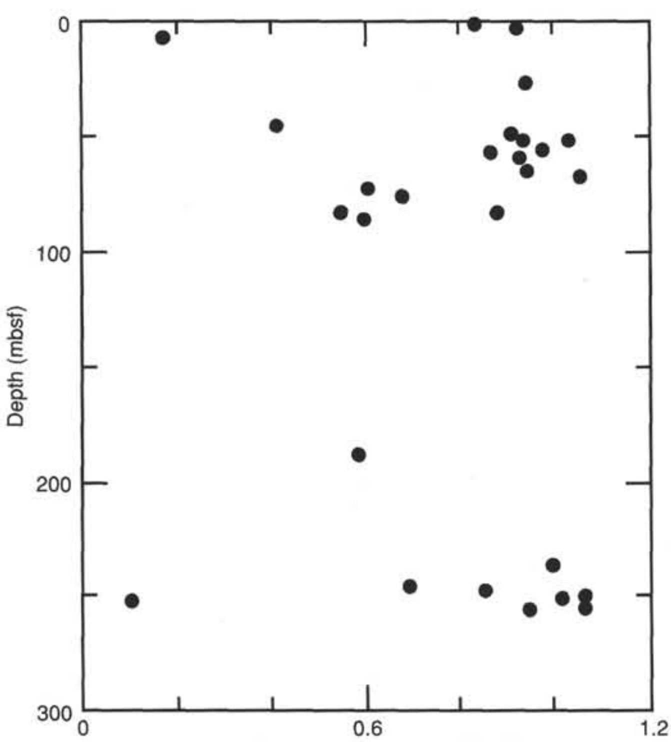

Figure 16. Plot of thermal conductivities vs. depth in Hole 781A. Note complete lack of correlation.

SUMMARY AND CONCLUSIONS

Site 781 lies on the lowermost flank of Conical Seamount about 7 nmi northwest of its summit. This site was chosen on the basis of a strong reflector at about 60 mbsf that was identified during a site survey and confirmed by a short shipboard seismic survey. Drilling at one RCB hole (Hole 781A) penetrated 250 m and recovered 39.6 m of core for a recovery rate of 16% (Fig. 21). Most of the poor core recovery was in sediments below basalt, which was encountered between 72.6 and 91.8 mbsf.

One lithostratigraphic unit having three subunits has been defined at Site 781 as follows:

1. Subunit IA (0–72.32 mbsf) comprises upper Pliocene to Holocene(?) diatom-radiolarian silty-clay grading downward into vitric silty clay and vitric clayey silt.
2. Subunit IB (72.32–91.80 mbsf) is a vesicular, porphyritic basalt.
3. Subunit IC (91.80–250 mbsf) comprises upper Pliocene to lower Pliocene vitric silty clay and vitric clayey silt.

Structures within the sediments in Subunit IA indicate deposition from gravity-driven mass flows. At least 19 turbidite sequences were identified with thicknesses ranging between 1 and 180 cm and with an average of 3 to 12 cm. Subunit IC contains lithologies similar to the lower part of Subunit IA, although poor recovery precludes detailed interpretation. Ages have been assigned on the basis of nannofossil and foraminifer assemblages in both Subunits IA and IC,

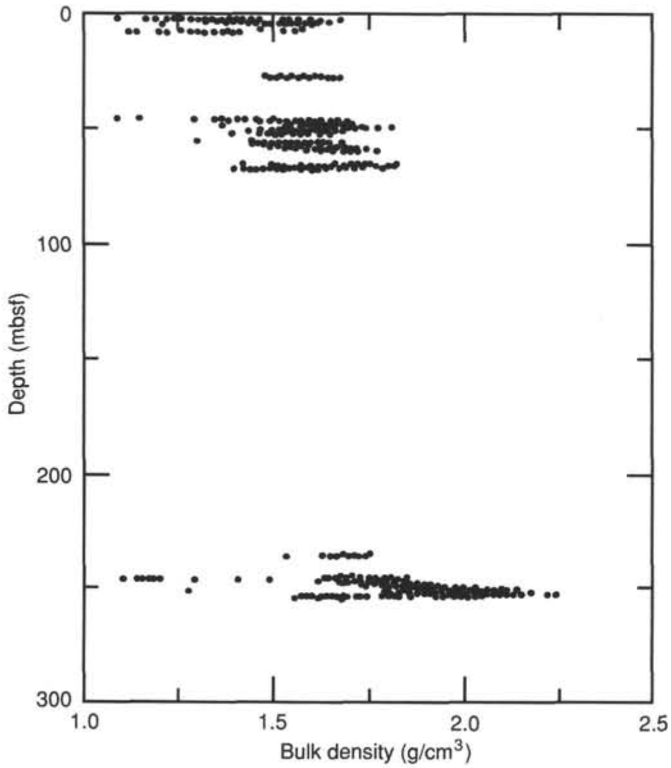

Figure 17. Plot of bulk densities (from the GRAPE sensor) vs. depth in Hole 781A. Bulk densities increase from approximately 1.4 to 2.0 g/cm^3 from the top to the bottom.

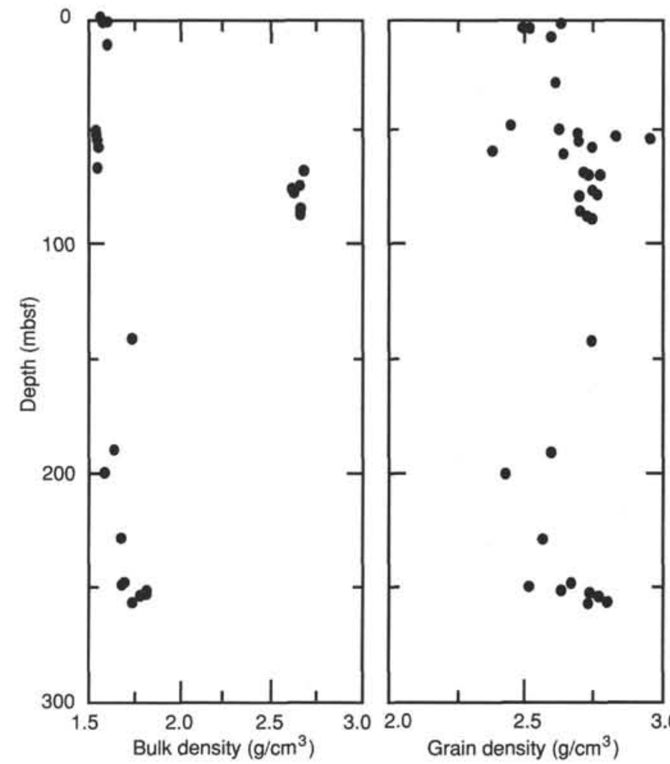

Figure 19. Variation of bulk and grain densities with depth in Hole 781A.

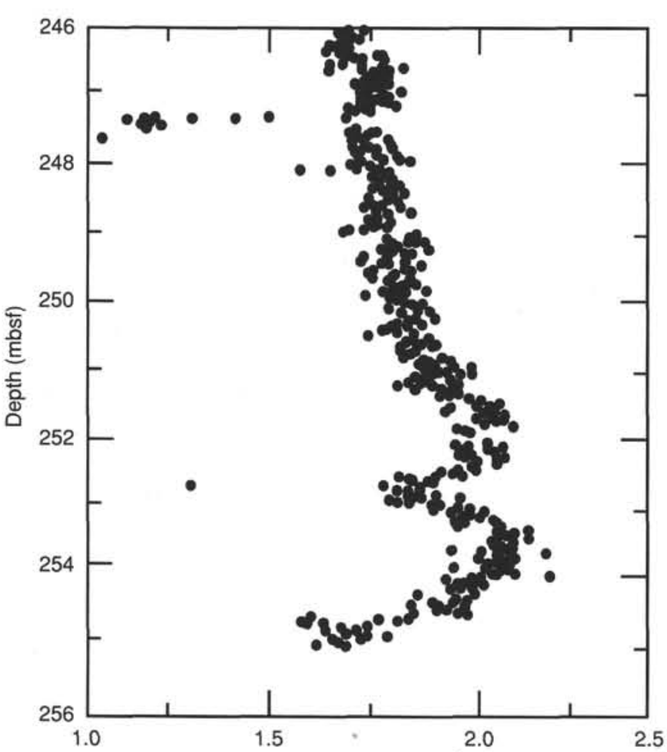

Figure 18. GRAPE bulk densities from the lowermost portion of Core 125-781A-27R (compare to Fig. 15 in "Paleomagnetism" section, this chapter). The increase in density is most probably related to metal filings and drill cuttings.

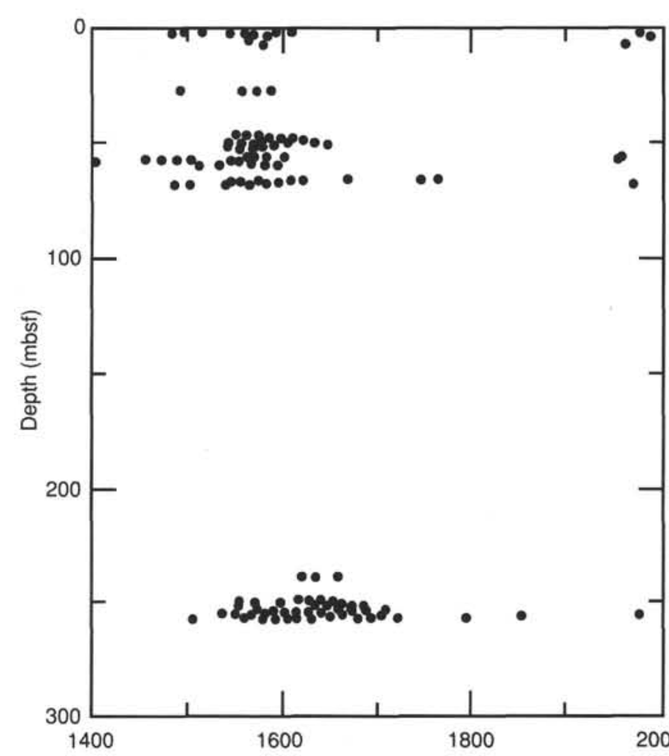

Figure 20. Plot of compressional-wave velocities (from velocity logger) vs. depth in Hole 781A. The increase in velocity is correlative to the increase in bulk density seen by GRAPE values.

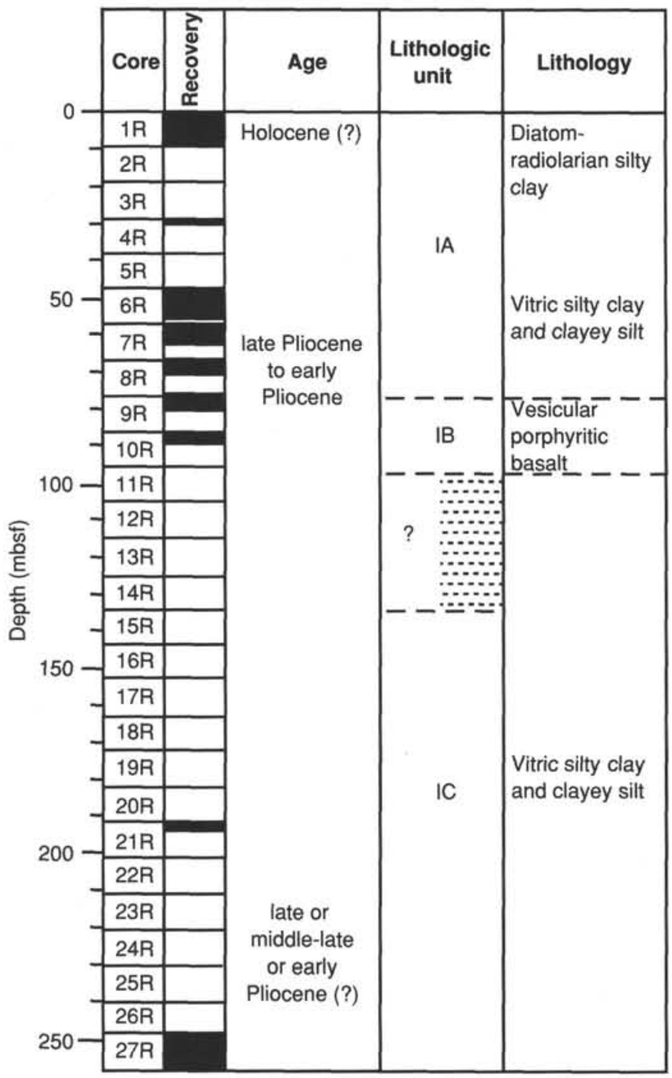

Figure 21. Core recovery and lithologic summary, Hole 781A.

although reworking, especially in Subunit IC, caused ambiguity.

Subunit IB, the cause of the reflector on the seismic records, is a 13- to 25-m-thick massive basalt containing up to 30% of phenocrysts and glomerocrysts of plagioclase, olivine, and clinopyroxene in a fine-grained groundmass. This basalt also contains from 2% to 10% of vesicles that increase in abundance and size toward the center of the subunit. The top of the basalt has an 8-mm-thick chilled margin that includes vesicle-free fresh glass. No internal flow boundaries exist in the recovered core. The basalt may be a near-surface sill or a lava flow: its reversed magnetic polarity, which contrasts with the normal polarity of the overlying sediments, is consistent with both possibilities.

Shipboard geochemical analyses of the basalt revealed that it was an island-arc tholeiite characterized by an enrichment in large-ion-lithophile elements relative to high-field-strength elements. This indicates that the magma originated from the mantle wedge above, and hence was modified by fluids from, the subducting lithosphere.

Studies of physical properties revealed high densities and magnetic susceptibilities in the sediments recovered in the final core. However, closer inspection showed that these properties could be explained by the presence of metal filings introduced during drilling of the last core while attempting to dry-drill for improved core recovery.

Unlike interstitial fluids from the summit and mid-flank of Conical Seamount, fluids from Site 781 exhibit only small chemical deviations from seawater composition downhole, which is more typical of a normal pelagic sequence.

In summary, the principal point of interest from Site 781 is the presence of a thick massive basalt of Pliocene or later age, the first evidence for such recent magmatic activity in any extant intraoceanic forearc terrane. The origin, provenance, and precise age of this basalt, when determined, will necessitate some revision of forearc models. The two main options are (1) that this basalt has been intruded laterally over a distance of about 100 km from the zone of active arc magmatism or (2) that it results from a hitherto unknown magmatic source within the forearc itself. A source in the convecting mantle beneath the subducting plate, however, can be considered unlikely on geochemical grounds.

REFERENCES

Berggren, W. A., Kent, D. V., Flynn, J. J., and Van Couvering, J., 1985. Cenozoic geochronology. *Geol. Soc. Am. Bull.*, 96:1407–1418.

McDuff, R. E., 1985. The chemistry of interstitial waters, Deep Sea Drilling Project Leg 86. *In* Heath, G. R., Burckle, L. H., et al., *Init. Repts. DSDP*, 86: Washington (U.S. Govt. Printing Office), 675–687.

Okada, H., and Bukry, D., 1980. Supplementary modification and introduction of code numbers to the low-latitude coccolith biostratigraphic zonation (Bukry, 1973, 1975). *Mar. Micropaleontol.*, 5:321–325.

Pearce, J. A., and Wanming, D., 1988. The ophiolites of the Tibetan Geotraverse, Lhasa to Golmud (1985) and Lhasa to Kathmandu (1986). *Phil. Trans. R. Soc. London*, A327:215–238.

Schneidermann, N., 1977. Selective dissolution of recent coccoliths in the Atlantic Ocean. *In* Ramsay, A.T.S. (Ed.), *Oceanic Micropalaeontology*, 2: London (Academic Press), 1009–1053.

Ms 125A-109

NOTE: All core description forms ("barrel sheets") and core photographs have been printed on coated paper and bound as Section 4, near the back of the book, beginning on page 383.